THE JOURNAL OF PHYSICAL CHEMISTRY B

Article

Cite This: J. Phys. Chem. B 2018, 122, 3339−3353

pubs.acs.org/JPCB

Alkali-Metal Trihalides: $M^+X_3^-$ Ion Pair or $MX-X_2$ Complex?

Zhi Sun,[†] Kevin B. Moore, III,[†] J. Grant Hill,[‡] Kirk A. Peterson,[§] Henry F. Schaefer, III,*[,†] and Roald Hoffmann*[,∥]

[†]Center for Computational Quantum Chemistry, University of Georgia, Athens, Georgia 30602, United States

[‡]Department of Chemistry, University of Sheffield, Sheffield S3 7HF, United Kingdom

[§]Department of Chemistry, Washington State University, Pullman, Washington 99164, United States

[∥]Department of Chemistry and Chemical Biology, Cornell University, Ithaca, New York 14853-1301, United States

Supporting Information

ABSTRACT: The alkali-metal trihalides MX_3 (M = Li, Na, K, Rb, and Cs; X = Cl, Br, and I) are systematically studied using coupled-cluster methods. Benchmarks using CCSD(T) against diatomic experimental results suggest satisfactory performance for the weighted core-valence basis sets (new basis sets for K, Rb, and Cs) selected for predicting reliable structures and harmonic vibrational frequencies. An isomer search using the B3LYP functional yields a planar, yet asymmetric T-shaped C_s structure as the global minimum for all MX_3 species. Much higher level CCSD(T) computations show a moderate to strong distortion of the X_3^- anion by the M^+ cation in the respective equilibrium geometries. Most obviously, for $LiCl_3$, the two Cl−Cl distances are separated by 0.786 Å. Even for CsI_3, the structure least distorted from the $M^+X_3^-$ model, the two I−I distances differ by 0.243 Å. It does not take much energy to distort the parent anions along an antisymmetric stretch, so this is no surprise. The normal modes of vibration of the MX_3 molecules are in better agreement with matrix isolation experiments than previous calculations. And these normal modes reveal that, instead of the well-established antisymmetric and symmetric stretches of the "free" X_3^- anions, relatively localized and mutually perturbed X−X and M−X stretches are calculated. The suggestion emerges that the MX_3 system may be alternatively described as an $MX-X_2$ complex rather than the $M^+X_3^-$ ion pair. This perspective is supported by bonding analyses showing low electron densities at the bond critical points and natural bond orders between the MX and X_2 moieties. The thermochemistry of fragmentations of MX_3 to MX + X_2 versus M^+ + X_3^- also supports the alternative viewpoint of the bonding in this class of molecules.

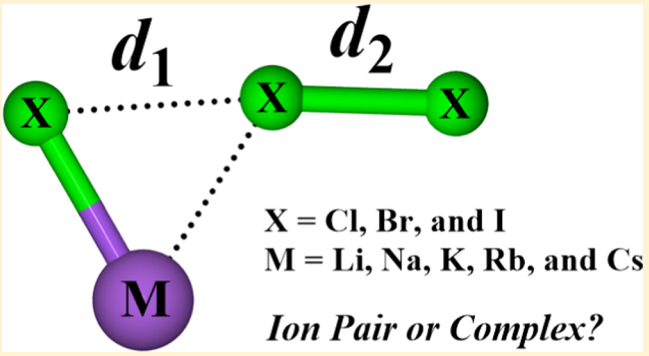

INTRODUCTION

There are only limited reports on the fundamental properties of alkali-metal trihalides, MX_3 (M = Li, Na, K, Rb, and Cs; X = F, Cl, Br, I). Among these, the four experimental papers on these halides in a noble gas matrix at low temperatures by Ault, Andrews, and co-workers are particularly important.[1−4]

All previous theoretical studies of MX_3 focused on the X_3^- properties and assumed the validity of an $M^+X_3^-$ ion pair model (M = Li, Na, K, Rb, and Cs).[1−4] The X_3^- anions have been considered as more or less "isolated" but perturbed by the M^+ cations. A recent theoretical study of the isolated halogen clusters X_3^- by Dixon and co-workers[5] is relevant to this situation. Early in the course of the present research, we realized that Dixon's computed harmonic vibrational frequencies (X−X−X symmetric and antisymmetric stretches) for the "free" Cl_3^- do not show satisfactory agreement with the IR/Raman frequencies of MCl_3 (M = Li, Na, K, Rb, and Cs) from the argon matrix experiments performed by Ault and Andrews.[3] Specifically, we note significant differences (up to 114 cm^{-1}, ∼30%) between the theoretical X_3^- and experimental MX_3 vibrational frequencies. It is thus uncertain if quantitative comparisons can be made between MX_3 and X_3^-. This leads to the question: is the perturbation due to an alkali cation strong enough to substantially change the electronic structures of the X_3^- and lead to significant modifications of these anions, in terms of structures, vibrational frequencies, and bonding?

The structures and frequencies of some MX_3 species in the solid state are known,[6,7] providing indications that the X_3^- moiety could be substantially altered by the presence of M^+. Instead of the well-established symmetric and antisymmetric stretches[3,5] for the free X_3^- anions, new modes with significant metal displacements may be involved in the MX_3 vibrations. Moreover, large red shifts (7−11%, about 20−60 cm^{-1}; see Table S1 in the SI) from gas phase to argon matrices are

Special Issue: Benjamin Widom Festschrift

Received: October 9, 2017
Revised: December 11, 2017
Published: December 12, 2017

DOI: 10.1021/acs.jpcb.7b10005
J. Phys. Chem. B 2018, 122, 3339−3353

highlighted by Jacox[8] for the ground-state vibrational fundamentals of diatomic alkali-metal halides (MX, M = Li, Na, K, Rb, Cs; X = F, Cl, Br, I). Similar red shifts can be also observed for the small MCl species involved in the experimental Ault and Andrews study of MCl_3 in argon (see Table S1 in SI).[3] If such red shifts carry over to the MX_3 species, it would impose challenges to achieving good agreement for the vibrational frequencies between gas-phase theoretical computations[5] and the argon matrix experiments.[1−4] And the solid-state compounds are bound to differ as well.

The solid-state and noble gas matrix perturbations we just mentioned are indicative of a more general truth: Even if we limit ourselves to an MX_3 stoichiometry, with M an alkali metal, the richness of experimental chemistry provides us with a good number of realizations of this formula. These include M^+ and X_3^- noninteracting in the gas phase, MX_3 molecules in a collisionless molecular beam, and MX_3 in a noble gas matrix, in solvents of varying polarity, in solids, and at surfaces and interfaces. This is hardly an exhaustive list of chemical and physical settings. Each situation will have a different (slightly, significantly) vibrational spectrum for MX_3 and an associated temperature. The studies we present here are, strictly speaking, for isolated MX_3 molecules, at $T \rightarrow 0$ K.

For the purpose of comparison, let us review the studies of free trihalide anions (X_3^-, X = F, Cl, Br, and I). These have been widely explored by both experiment and theory, in the gas phase,[9,10] solution,[11,12] and solid state.[13,14] Those species have been well characterized by IR and Raman spectra,[3,6,15−17] and some gas-phase thermochemistry of the X_3^- species has been reported.[9,10,18,19] In regard to previous theoretical research, a significant focus has been the interpretation of X_3^- electronic structure and bonding. Basically, all X_3^- species have been described as either (1) a 4-electron 3-center (4e-3c)[20−24] hypervalent bonding system using the Rundle−Pimentel model[25,26] or (2) a donor−acceptor interacting system between two closed-shell fragments X_2 and X^- (bonding types I and II in Scheme 1). Insights from molecular orbital theory are particularly relevant in this regard.[20,21] Hiberty and co-workers[22,23] employed valence bond theory to propose another three-electron bonding type (bonding type III in Scheme 1) as an important contributor to the electronic structure of F_3^-. This special bonding character of F_3^- has been used to discuss its exceptional multireference[27] and symmetry-breaking[28] challenges, as well as its peculiar preference of the energetically disfavored dissociation channel into F_2^- and $F^\bullet$ at high collision energies.[18]

Scheme 1. General Bonding Types Proposed for the 4-Electron 3-Center Hypervalent X_3^- (Bonding Types I and II for Cl_3^-, Br_3^-, and I_3^-; Types I, II, and III for F_3^-) Systems

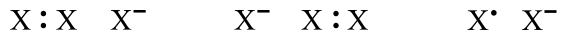

(I) (II) (III)

Direct theoretical studies of MX_3 species have been generally limited to the fluoride systems.[29−31] The structures, vibrational frequencies, and dissociation energies of MF_3 (M = Na, K, Rb, and Cs) were systematically studied by Tozer and Sosa[29] as early as 1997 using Hartree−Fock, MP2, QCISD, BLYP, and B3LYP methods. The results were found to be strongly dependent on the identity of the metals, as well as the theoretical methods applied. The method dependence emerged in locating the true minima and corresponding vibrational frequencies, with only the B3LYP functional predicting the metal-dependent minima (Na: C_s isomer; K, Rb, and Cs: C_{2v} isomer, see Figure 1) inferred from the IR/Raman spectra by Andrews and co-workers.[32,33] The C_{2v} isomers for KF_3 and CsF_3 have been more recently (2015) studied using CCSD-(T)/def2-TZVPP computations by Riedel and co-workers.[31] The MF_3 (M = Li, Na, and K) species were also studied in 2015 using the CCSD(T)/6-311+G(3df) method by Getmanskii et al.[30]

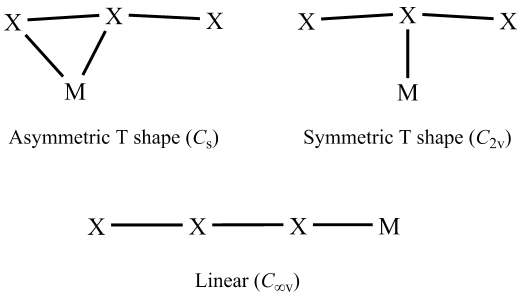

Figure 1. Structures of MF_3 (M = Li, Na, K, Rb, and Cs) reported in the literature.[29−31]

Minima for all three isomers sketched in Figure 1 were located for all three fluoride species, except that the asymmetric T-shaped minimum was not found for KF_3. The global minima for LiF_3 and NaF_3 were found to be the asymmetric and symmetric T-shaped structures, respectively. However, a tiny 0.16 kcal mol^{-1} (zero-point vibrational energies (ZPVE)-corrected) energy difference between the two T-shaped NaF_3 structures introduces additional uncertainties. The general preference of the C_{2v} global minimum for MF_3 could originate from the special electronic structure of F_3^- discussed above (see Scheme 1). Because the heavier X_3^- anions do not possess this unique F_3^- electronic structure, it is unclear if such structural preferences also occur for other alkali-metal trihalides, MX_3 (X = Cl, Br, and I).

There are limited theoretical and experimental results for the heavier halides MX_3 (X = Cl, Br, and I), and it would be beneficial to probe the latter species with rigorous computations. The present study does this and aims to offer some answers to the following questions:

(1) Why is the agreement between theoretical[5] X_3^- and experimental[3] MX_3 vibrational frequencies relatively unsatisfactory?
(2) Could the metal-dependent global minima found[29,30] for MF_3 also occur for MCl_3, MBr_3, and MI_3?
(3) What are the differences between X_3^- and MX_3 in terms of structures, vibrational modes and frequencies, bonding characters, and thermochemistry?
(4) Finally, the title question, not anticipated, but one that arose quite naturally as we progressed: should the alkali-metal trihalides be described as ion pairs between M^+ and X_3^- or as complexes between MX and X_2?

THEORETICAL METHODS

An isomer search for the MX_3 global minima was conducted by optimizing various prospective structures using the B3LYP3 functional[34−36] implemented in MOLPRO 2010.1.[37,38] This particular version of the B3LYP functional utilizes the standard VWN3 local correlation energy parameters.[34] For these

DOI: 10.1021/acs.jpcb.7b10005
J. Phys. Chem. B 2018, 122, 3339−3353

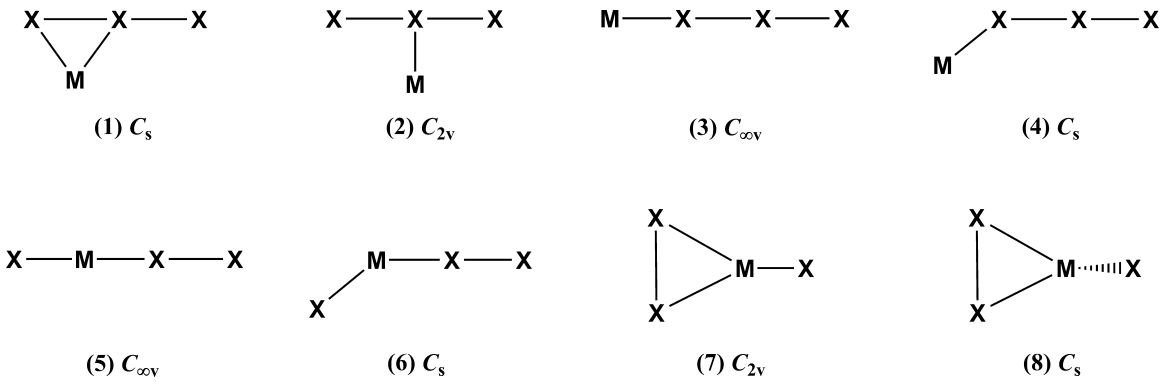

Figure 2. Possible stationary point structures explored for the MX_3 (M = Li, Na, K; X = Cl, Br, I) systems using B3LYP/AVTZ method.

computations, the SCF energies and densities were both converged to 10^{-10} and the root mean square (RMS) force was converged to 10^{-8} Hartree Bohr^{-1}. Stationary points obtained from these optimizations were classified by their harmonic vibrational frequencies, obtained via finite differences of analytic energy gradients. The following standard correlation-consistent valence basis sets (AVTZ for simplicity) were used in the density functional theory (DFT) computations

Li, Na: cc-pVTZ[39]
K, Rb, Cs: cc-pVTZ-PP[40]
Cl: aug-cc-pVTZ[41]
Br, I: aug-cc-pVTZ-PP[42]

The equilibrium geometries, harmonic vibrational frequencies, and dissociation energies (D_0) of MX_3 global minima were subsequently obtained (with new and different core-correlated basis sets) using coupled-cluster theory with single, double, and perturbative triple excitations [CCSD(T)],[43−46] as implemented in CFOUR 2.0.[47,48] The restricted Hartree−Fock method was used throughout, as all of the species of interest are closed-shell. For all CCSD(T) computations, the SCF densities, CC amplitudes, and λ coefficients are converged to 10^{-10}. The RMS force of the geometries was converged to 10^{-8} Hartree Bohr^{-1}. The gradients were obtained via analytic first derivatives of the CCSD(T) energy, and the frequencies were obtained by finite differences of these gradients. Listed below is a new group of weighted core-valence basis sets (AWCVTZ for simplicity) that was used for the CCSD(T) computations:

Li, Na: cc-pwCVTZ[39]
K, Rb, Cs: cc-pwCVTZ-PP[40]
Cl: aug-cc-pwCVTZ[41,49]
Br, I: aug-cc-pwCVTZ-PP[50,51]

These are correlation-consistent (cc), polarized (p), weighted core-valence (wCV), and triple-zeta (TZ) basis sets. Each halogen atom (Cl, Br, I) basis set is augmented with additional diffuse basis functions to describe potential anionic character. All electrons of the Li, Na, and Cl atoms were correlated in the CCSD(T) computations. For K, Rb, Cs, Br, and I, deep inner electrons were treated by effective core potentials (described below). This method was chosen because the traditional frozen-core approximation yielded several errors in the optimized structures and harmonic vibrational frequencies for certain species (e.g., KCl_3). These issues appear to stem from systems having correlated and uncorrelated molecular orbitals with nearly degenerate energies. Further wavefunction diagnostics provided in the SI demonstrate that our chosen single-reference CCSD(T) methods should be reliable. All energy and property computations were performed using the CCSD(T)/AWCVTZ structures.

For both the B3LYP and CCSD(T) computations, we employ the multiconfigurational Dirac Hartree−Fock fit, fully relativistic Köln/Stuttgart effective core potentials (ECPs) to model the inner core electrons of the atoms below the third row [ECP10MDF (K and Br): 10 electrons ($1s^2 2s^2 2p^6$); ECP28MDF (Rb and I): 28 electrons ($1s^2 2s^2 2p^6 3s^2 3p^6 3d^{10}$); and ECP46MDF (Cs): 46 electrons ($1s^2 2s^2 2p^6 3s^2 3p^6 4s^2 3d^{10} 4p^6 4d^{10}$)].[52] For the atoms treated by an ECP, the corresponding -PP basis sets are used. Because the cc-pVTZ-PP and cc-pwCVTZ-PP basis sets for K, Rb, and Cs are not yet available in the literature, we have provided them in the Supporting Information (SI). These basis sets are specifically matched to the ECPs mentioned above and have the following number of primitives and contracted functions at the cc-pVTZ-PP level: K, (11s10p6d1f)/[5s4p3d1f]; Rb, (11s9p5d1f)/[5s4p3d1f]; and Cs, (11s9p6d4f)/[5s4p3d2f]. In all cases, linear dependency issues were avoided by constraining the optimizations such that the ratio between successive functions in a given angular symmetry was greater than or equal to 1.6. The problem of correlating functions in ECP-based calculations recovering less correlation energy than in all-electron calculations[53,54] was circumvented by uncontracting an extra s-type correlating function, as in previous work.[54,55] The cc-pwCVTZ-PP basis sets for these elements add 2s2p2d1f sets of functions that have been optimized using the well-established strategy for weighted core-valence basis sets.[49] To keep discussions throughout the main text succinct, we will refer to the mixture of these basis sets for the B3LYP and CCSD(T) simply as AVTZ and AWCVTZ, respectively.

A bonding analysis of the optimized MX_3 species was performed using Weinhold natural bond orbital (NBO) theory[56] and the Bader quantum theory of atoms in molecules (QTAIM).[57] Intermolecular hyperconjugation was quantified with the second-order energy for delocalizing electrons from a donor orbital (L) to an acceptor orbital (NL)[58]

$$E(2) = q_L \frac{F(L, NL)^2}{\varepsilon_{NL} - \varepsilon_L}$$

where F(L, NL) is the NBO Fock matrix element and q_L and ε_L are the occupancy and energy of orbital L, respectively. Resonance structures from natural resonance theory[59−61] were obtained to characterize the overall electronic structure and types of bonding in MX_3. We expand this picture by discussing the covalent and ionic contributions to the natural bond order. QTAIM was used to locate the bond critical points to assess the

DOI: 10.1021/acs.jpcb.7b10005
J. Phys. Chem. B 2018, 122, 3339−3353

Table 1. Benchmark of the CCSD(T)/AWCVTZ Equilibrium Bond Lengths (in Å) and Harmonic Vibrational Frequencies (in cm^{-1}) of MX and X_2 (M = Li, Na, K, Rb, and Cs; X = Cl, Br, and I) Molecules Against Experimental Values from the NIST Tables

	equilibrium bond lengths				harmonic vibrational frequencies		
species	computed	NIST	deviation	percent error (%)	computed	NIST	percent error (%)
LiCl	2.029	2.021	0.008	0.4	635	643	−1.2
NaCl	2.373	2.361	0.013	0.6	359	366	−1.9
KCl	2.683	2.667	0.017	0.6	276	281	−1.8
RbCl	2.805	2.787	0.019	0.7	231	228	1.3
CsCl	2.939	2.906	0.033	1.1	210	214	−1.9
LiBr	2.180	2.170	0.009	0.4	553	563	−1.8
NaBr	2.517	2.502	0.015	0.6	293	302	−3.0
KBr	2.838	2.821	0.018	0.6	216	213	1.4
RbBr	2.964	2.945	0.020	0.7	167	169	−1.2
CsBr	3.104	3.072	0.032	1.0	147	150	−2.0
LiI	2.400	2.392	0.008	0.3	493	498	−1.0
NaI	2.729	2.711	0.018	0.7	254	258	−1.6
KI	3.066	3.048	0.019	0.6	184	187	−1.6
RbI	3.199	3.177	0.023	0.7	136	139	−2.2
CsI	3.348	3.315	0.033	1.0	117	119	−1.7
Cl_2	2.003	1.987	0.016	0.8	548	560	−2.1
Br_2	2.295	2.281	0.014	0.6	319	325	−1.8
I_2	2.673	2.666	0.007	0.3	217	215	0.9
		mean:	**0.018**	**0.7**		**mean:**	**1.7**

electron density occurring between each atom. The above described NBO (HF/AWCVTZ) and QTAIM (B3LYP/AVTZ) analyses were performed using NBO 6.0[58] and AIMAll 16.01.09.[62]

RESULTS AND DISCUSSION

A systematic study of MX_3 (M = Li, Na, K, Rb, and Cs; X = Cl, Br, and I) was performed using density functional and coupled-cluster methods. In view of possible metal dependence indicated by theoretical studies of MF_3 (M = Li, Na, K, Rb, and Cs),[29−31] several structures were considered (Figure 2) using the B3LYP functional to locate possible local minima. This was then followed by high-level coupled-cluster computations [CCSD(T) with the weighted core-valence basis sets, see Theoretical Methods]. The equilibrium geometries (Table 2 and Figure 3), vibrational modes and frequencies (Tables 3−6 and Figure 5), bond analysis (Table 7), thermochemistry (Table 8), and other relevant results for each species considered are reported and discussed.

Performance of the New Weighted Core-Valence Basis Sets. We wish to assess the uncertainty of the computed geometries and vibrational frequencies for the MX_3 species. In addition, the weighted core-valence basis sets for the alkali metals (K, Rb, and Cs, see Theoretical Methods and SI) are newly developed, and little assessment of their accuracy is currently available (see, however, ref 40). Because there is little experimental information on the MX_3 species, the relevant diatomic species MX and X_2 (M = Li, Na, K, Rb, Cs; X = Cl, Br, I) are selected as a test set. Within the NIST database,[63] there are well-established gas-phase experimental values for the equilibrium bond distances and harmonic vibrational frequencies of MX and X_2. Within this test set, 15 ionic and 3 covalent bonds are included, and we benchmark our chosen theoretical methods against the experimental values of these species in Table 1.

For the equilibrium bond length, the overall mean absolute error and mean absolute percent error were found to be 0.018 Å and 0.7%, respectively. For each of the three metal halide series (MCl, MBr, and MI), the theoretical bond lengths are all slightly longer than the experimental values, with an increasing trend from LiX to CsX. The largest differences between theory and experiment occur for CsX, with percent errors being 1.1, 1.0, and 1.0% for CsCl, CsBr, and CsI, respectively. For X_2 (X = Cl, Br, and I), a decreasing trend in positive deviations (Cl_2: 0.8%; Br_2: 0.6%; and I_2: 0.3%) can be noted.

For the harmonic vibrational frequencies, the overall mean absolute percent error was found to be 1.7%. From Table 1, most deviations are negative and within 2.0%. However, RbCl, KBr, and I_2 are exceptions with positive deviations, and NaBr is the species with the highest deviation beyond 2.0% (−3.0%). No obvious trend in percent errors can be found for the MCl and MBr series; however, the MI series shows an increasing trend from LiI to RbI, with an exception that the percent error for CsI drops below RbI. Consistent with the situation for bond lengths, the percent errors of the X_2 species decrease from Cl_2 to I_2 (Cl_2: −2.1%; Br_2: −1.8%; and I_2: 0.9%).

In summary, the CCSD(T) method with the selected weighted core-valence basis sets predicts reliable structures and harmonic frequencies for the relevant diatomic species MX and X_2 (M = Li, Na, K, Rb, Cs; X = Cl, Br, I). Accordingly, the accuracy of our computed equilibrium bond lengths and harmonic vibrational frequencies of alkali-metal trihalides MX_3 should be satisfactory for assessing the experimental conclusions of Ault, Andrews, and co-workers.[3]

Possible MX_3 Structures. Previous theoretical[29−31] and experimental studies[32,33] have shown that the identity of the metal (M) in the metal fluoride systems MF_3 (M = Li, Na, K, Rb, and Cs) dictates the structure of the global minimum. To investigate whether a similar metal dependence exists for MX_3 (M = Li, Na, K, Rb, Cs; X = Cl, Br, I) species, several structures were first considered using the B3LYP/AVTZ method. The B3LYP functional was selected due to its reliable performance in the theoretical fluoride study of Tozer and Sosa[29] in reproducing Ault and Andrews's MF_3 experimental results.[32,33]

DOI: 10.1021/acs.jpcb.7b10005
J. Phys. Chem. B 2018, 122, 3339−3353

Table 2. Equilibrium Geometries (Bond Lengths in Å and Angles in Degrees) of MX_3 (M = Li, Na, K, Rb, and Cs; X = Cl, Br, and I) Minima (See Figure 3) Optimized Using the CCSD(T)/AWCVTZ Method[a]

species	B1(X1−X2)	B2(X2−X3)	B3(M−X1)	B4(M−X2)	A(X1−X2−X3)	A(X1−M−X2)
Cl_3^-	2.313 (2.314[b], 2.313[c])	2.313 (2.314[b], 2.313[c])			180.0	
$LiCl_3$	2.836	2.050	2.079	2.382	169.1	78.6
$NaCl_3$	2.719	2.078	2.440	2.733	174.1	63.1
KCl_3	2.598	2.116	2.786	2.982	174.3	53.4
$RbCl_3$	2.569	2.127	2.925	3.096	174.1	50.4
$CsCl_3$	2.553	2.132	3.084	3.253	174.1	47.4
Br_3^-	2.571 (2.585[b])	2.571 (2.585[b])			180.0	
$LiBr_3$	2.879	2.385	2.269	2.463	171.0	74.8
$NaBr_3$	2.817	2.410	2.629	2.809	174.0	62.3
KBr_3	2.741 (2.64[d])	2.441 (2.49[d])	2.989	3.083	173.2	53.6
$RbBr_3$	2.721	2.450	3.137	3.199	172.7	50.9
$CsBr_3$	2.702 (2.698[e])	2.458 (2.440[e])	3.312	3.344	172.0	47.9
I_3^-	2.944 (2.972[b], 2.945[f])	2.944 (2.972[b], 2.945[f])			180.0	
LiI_3	3.229	2.769	2.504	2.664	170.2	77.3
NaI_3	3.182	2.790	2.855	3.017	173.4	65.6
KI_3	3.113	2.816	3.226	3.321	172.9	56.8
RbI_3	3.095 (3.051[g])	2.824 (2.833[g])	3.376	3.444	172.4	54.0
CsI_3	3.075 (3.03[h])	2.832 (2.83[h])	3.552	3.589	171.7	51.0

[a]Previously reported values are given in parentheses. [b]The CCSD(T)/aug-cc-pV(T+d)Z values from ref 5. [c]The CCSD(T)/aug-cc-pVQZ values from ref 64. [d]X-ray values of *Pnma* KBr_3 crystal from ref 66. [e]X-ray values of *Pmnb* $CsBr_3$ crystal from ref 67. [f]The CCSD(T)/aug-cc-pVTZ-PP values from ref 23. [g]X-ray values of *Pnma* RbI_3 crystal from ref 68. [h]X-ray values of CsI_3 crystal from refs 69, 70.

The isomers explored for the MX_3 (M = Li, Na, K; X = Cl, Br, I) are shown in Figure 2. The first three structures (also shown in Figure 1) were chosen because they have been previously identified as minimum-energy structures on the MF_3 potential energy surface.[29−31] Five additional structures (**4**−**8** in Figure 2) were selected as they represent alternate symmetries, which are constrained during optimization. Also the coplanarity of all four atoms implicit in structures **1** and **2** was relaxed, effectively allowing **1** to be C_1 and **2** C_s in symmetry.

In contrast to the structural variations noted in the case of the fluoride species MF_3,[29,30] results for the other halides, the subject of this study, are generally consistent for Li, Na, and K. For all MX_3 species, structures **1**, **2**, and **3** correspond to minima, transition states, and second-order saddle points, respectively. The only other possible minimum was found to be the structure **7**, although it shows some metal dependence. The LiX_3 structures **7** were all found to be first-order saddle points with small imaginary frequencies of 43i, 34i, and 22i cm^{-1} for $LiCl_3$, $LiBr_3$, and LiI_3, respectively. Most NaX_3 and KX_3 structures of type **7** were predicted to be minima. However, a tiny imaginary frequency (5i) and two small imaginary frequencies (20i and 12i) were predicted for $NaCl_3$ and KBr_3, respectively. Finer integration grids might predict all real frequencies for these species, but the long interfragment distance (2.5−3.5 Å) and the small first few frequencies (below 50 cm^{-1}) indicate that the structure **7** is not a strongly bound minimum. Moreover, for all MX_3 species investigated, structure **7** lies 5.9−15.2 kcal mol^{-1} above structure **1** at the ZPVE-corrected B3LYP level. Optimizations of structures **4**, **6**, and **8** lead to either structure **1** or **7** (see SI). Optimizations of structure **5** separated the MX and X_2 moieties beyond 4.0 Å.

Could structures **1** and **2** be nonplanar (as one sees in the trifluorides)? Optimizations begun in nonplanar geometries returned uniformly to C_s and C_{2v} minima. There were two exceptions: 1. For MCl_3 (M = Na, K, Rb, Cs), a noncoplanar structure derived from **2** was a stationary point that turned out to be a transition state; the large imaginary frequency characterizing this geometry led to a structure **1** geometry. 2. For $CsBr_3$, a nearly planar structure close to C_{2v} (near **2**) was a minimum, with a low-frequency (23 cm^{-1}) mode leading back to structure **1**.

Although the C_s structures are definitely preferred, the question could be asked "by how much?" Some representative numbers for the energy difference between optimized C_s and C_{2v} structures are −11.0 kcal mol^{-1} for $LiCl_3$, 1.1 kcal mol^{-1} for $CsCl_3$, 10.0 kcal mol^{-1} for LiI_3, and 1.2 kcal mol^{-1} for CsI_3. For Li species, the C_s and C_{2v} structures are clearly separated by ∼10 kcal mol^{-1}. However, the CsX_3 (X = Cl or I) have C_s and C_{2v} structures that are nearly degenerate in energy, consistent with their small imaginary frequencies (55i and 16i for $CsCl_3$ and CsI_3, respectively) in their C_{2v} shape. This is an indication that large alkali metals (such as Cs) tend to have less impact on the X_3^- than the small ones (Li, for instance). We will explore this point further in the following sections.

In summary, the strong metal dependence reported for the MF_3 (M = Li, Na, K, Rb, and Cs)[29,30] species does not appear to carry over to the MX_3 (X = Cl, Br, and I) systems. In contrast to the general preference for a C_{2v} global minimum for MF_3, our DFT computations suggest that the asymmetric T-shaped C_s structure (structure **1** in Figure 2) is a global minimum for all MX_3 species. This is consistent with the Ault and Andrews's experimental finding for MCl_3 (M = Li, Na, K, Rb, and Cs).[3] We only focus on the asymmetric T-shaped global minimum for the rest of the discussion.

Equilibrium Geometries for MX_3. The labels of atoms and bonds in MX_3 (M = Li, Na, K, Rb, and Cs; X = Cl, Br, and I) are shown in Figure 3, and the parameters of all equilibrium geometries are listed in Table 2. For comparison, the free X_3^- (X = Cl, Br, and I) geometries are also reported.

DOI: 10.1021/acs.jpcb.7b10005
J. Phys. Chem. B 2018, 122, 3339−3353

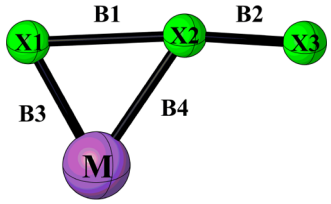

Figure 3. Labels of atoms and bonds in MX_3 (M = Li, Na, K, Rb, and Cs; X = Cl, Br, and I) used in Table 2.

For the trihalide series seen in Table 2, the Cl−Cl bond distance in the free Cl_3^- ($D_{\infty h}$) is predicted to be 2.313 Å at the CCSD(T)/aug-cc-pwCVTZ level. This value agrees well with the CCSD(T)/aug-cc-pV(T+d)Z result (2.314 Å) by Dixon and co-workers[5] and the CCSD(T)/aug-cc-pVQZ result (2.313 Å) by Riedel et al.[64] The Br−Br bond distance in Br_3^- is predicted to be 2.571 Å at the CCSD(T)/aug-cc-pwCVTZ-PP level. This value is slightly shorter than the Br−Br distance (2.585 Å) computed at the CCSD(T)/aug-cc-pVTZ-PP level by Dixon and co-workers.[5] Both Cl−Cl and Br−Br bond distances are also close to DFT results obtained at the MPWB1K/6-31+G(d) level of theory by Pichierri.[65] The I−I bond distance in free I_3^- is predicted to be 2.944 Å at the CCSD(T)/aug-cc-pwCVTZ-PP level. This value is shorter than the I−I distance (2.973 Å) computed with the CCSD(T)/aug-cc-pVTZ-PP method by Dixon and co-workers.[5] However, our distance agrees well with the result (2.945 Å) at the CCSD(T)/aug-cc-pVTZ-PP level (all orbitals are correlated) by Braïda and Hiberty.[23] The difference in bond lengths calculated with ostensibly the same methodology, not to speak of what would be obtained with different levels of calculation, serves in a way to set the theoretical equivalent of an error bar on a calculation.

There are to date limited reports of any type for the MX_3 (X = Cl, Br, and I) structures in the gas phase or in matrices. Hence, we are drawn to some solid-state results. And here we need to insert an anticipation of what Table 2 holds, which can be summarized as a variable asymmetrization of the trihalide moiety of MX_3, in the asymmetric environment the trihalide faces in a C_s geometry.

Such asymmetrization is a sign of the relatively small energy involved in changing the *B*1 and *B*2 bond lengths from equality in X_3^- itself, no cation present, along an antisymmetric stretching coordinate. Experimentally, the evidence for this is the beautiful Bürgi and Dunitz diagram (a plot of *B*1 vs *B*2) for all of the triiodide structures in the Cambridge Structural Database (CSD[71]) in 2003, by Svensson and Kloo.[72] We have regenerated this plot in Figure 4. The impetus for a structure to move from the 45° line (*B*1 = *B*2) is, of course, the asymmetry of the countercation in the structure, or the crystal packing. Whichever it is, the hyperbola we see is prima facie evidence of an energetically easy excursion along a very specific potential energy surface in which *B*1 ≠ *B*2. A similar diagram for tribromide structures may be found in Robertson et al.[14]

We can simulate the energetics involved theoretically by fixing 2.67 Å < *B*1 < 2.94 Å (the limits are its values in I_2 and I_3^-), and allowing *B*2 to vary. The resulting plot (in the SI) reproduces the hyperbola pretty well and shows that it takes 4.8 kcal mol^{-1} for I_3^- to move from *B*1 = 2.67 Å, *B*2 = 3.07 Å to *B*1 = *B*2 = 2.94 Å.

Returning to specifically MX_3 structures, with the M of this study, we do find some in the literature. In these, even if the stoichiometry is MX_3, one does not have a molecular crystal of

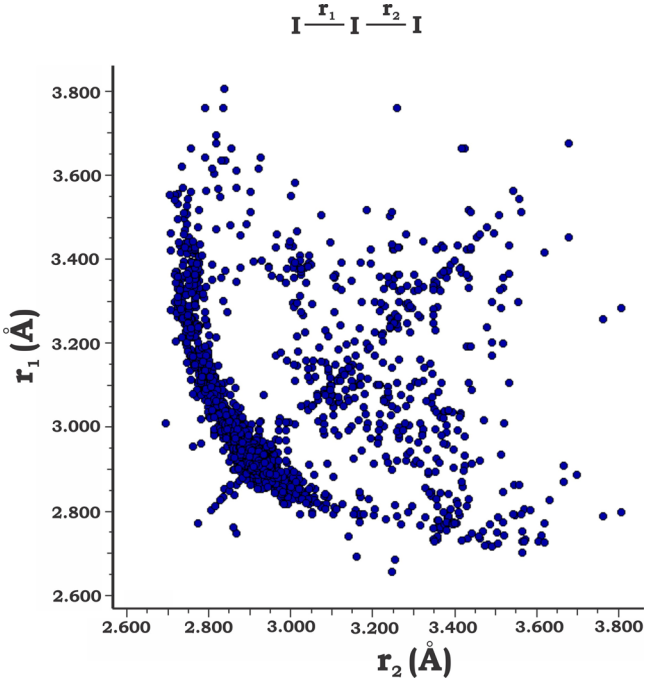

Figure 4. Plot of the two distances, *r*1 and *r*2 (corresponding to our *B*1 and *B*2) in the triiodide structures in the Cambridge Structural Database. Reprinted from ref 74. Copyright 2013 American Chemical Society.

MX_3 entities well separated from other such molecules; instead there are arrangements of varying complexity of X_3 anions of varying asymmetry, and the M cations.

The structures observed fall into three groups: (1) MX_3 solid-state structures; (2) $MX_3{\cdot}Z$, where one or more Z molecules accompany the metal halide in the solid-state structure; and (3) extended structures associated with high-pressure environments, often theoretical.

In group 1, we have structures of $CsBr_3$, RbI_3, and CsI_3 (the latter done independently by two groups, and also at −160 °C).[67,68,70,73] In each case, the coordination environment of the trihalide is far from simple; for instance, in $CsBr_3$, the tribromide group has no less than eight different Cs^+ ions coordinated to it, at 3.52−4.02 Å. And that coordination environment is very different from that we calculate for our isolated MX_3 molecules. Nevertheless, the observed asymmetries of the trihalides in these structures quite remarkably resemble those calculated by us for isolated molecules. In the crystal structure of $CsBr_3$ in *Pmnb* space group,[67] the experimental Br−Br bond length pair was reported to be 2.698/2.440 Å, which agrees well with the values 2.702/2.458 Å reported in the present research. The I−I bond length pairs in the RbI_3[68] and CsI_3[69,70] crystal structures were reported to be 3.051/2.833 and 3.04/2.84 Å (some variation among the crystal structures), respectively, and the two sets of values are close to the corresponding 3.095/2.824 and 3.075/2.832 Å obtained at the CCSD(T)/AWCVTZ level in this work. A theoretical study of the CsI_3 crystal finds 3.01/2.90 Å.[75]

The second group, MX_3, associated with other molecules, is a rich one. Here are three examples of many: $KI_3{\cdot}H_2O$, $KI{\cdot}KI_3{\cdot}6$(*N*-methyacetamide), and $Cs_2I_8 = Cs_2{\cdot}(I_3)_2{\cdot}I_2$.[76−78] Naturally, the triiodide environments are still more complex in these compounds. Remarkably, the triodide in $KI_3{\cdot}H_2O$ is nearly symmetrical, I−I 2.925/2.935 Å, the asymmetry calculated by

DOI: 10.1021/acs.jpcb.7b10005
J. Phys. Chem. B 2018, 122, 3339−3353

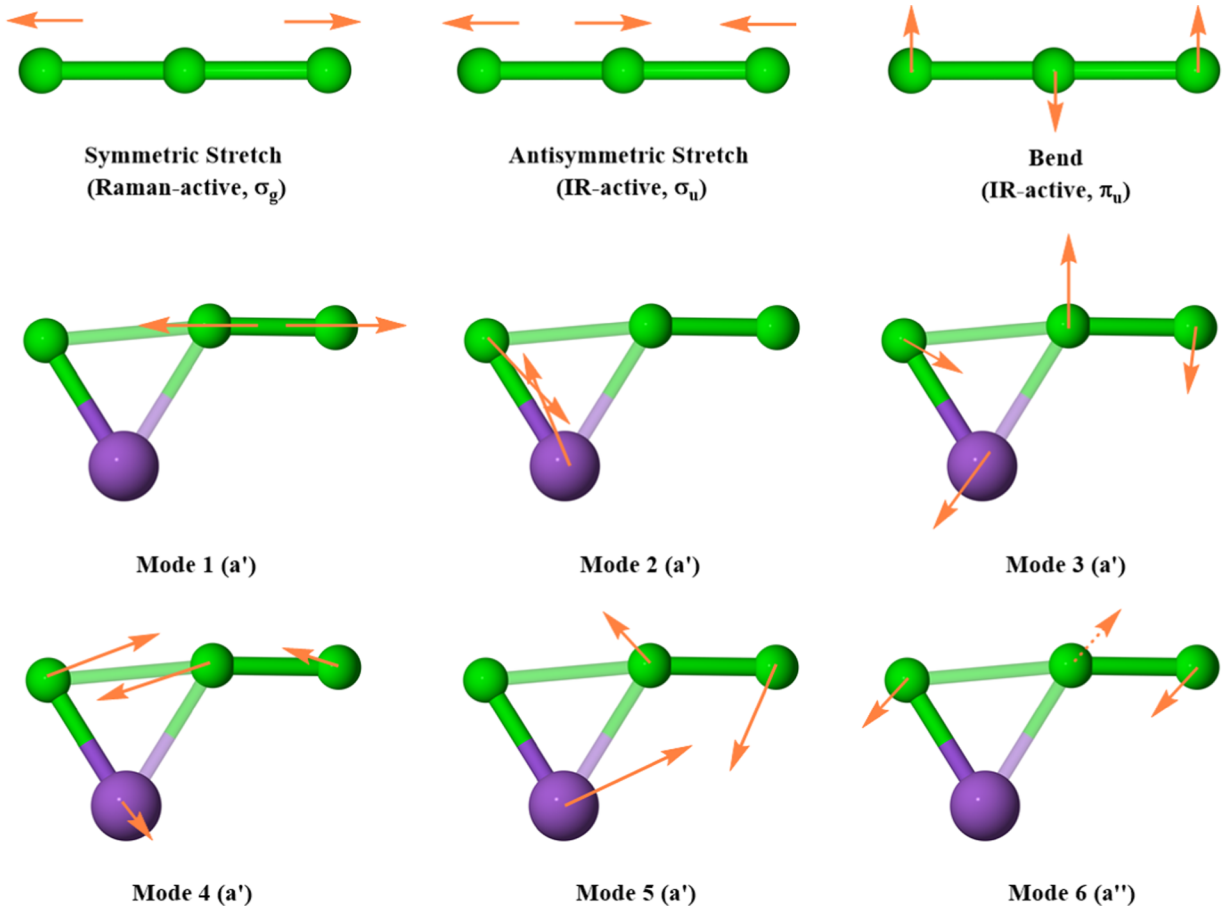

Figure 5. Vibrational modes for the $D_{\infty h}$ free X_3^- (illustrated for Cl_3^-) and C_s MX_3 (illustrated for KCl_3).

us is 2.816/3.182 Å. The trihalides in Cs_2I_8 are closer to our molecular asymmetry, at 2.84/3.00 Å. One has to draw an imaginary line somewhere in listing compounds in this class, as the structures quickly shade over to the multitudinous class of polyiodides, in which trihalides interact weakly or strongly with iodide ions and I_2 molecules.[72]

The high-pressure structures, the third group, are a relatively new phenomenon, one with which one of us (RH) is much involved. Under extreme conditions of elevated pressure, new stoichiometries emerge, simply not there at 1 atm. Calculations often precede syntheses in this playground; actual observation of predicted phases is relatively rare. In the two cases we mention, $NaCl_3$ and KCl_3, one actually has seen the compositions in experiment. In the $NaCl_3$ crystal structure (*Pm*3*n* space group) at high pressure (200 GPa),[79] the shortest Cl−Cl and Na−Cl bond distances have been recently reported to be 2.06 and 2.30 Å, respectively. These two distances are not far from 2.078 and 2.440 Å (*B*2 and *B*3 in Figure 3 and Table 2) at the CCSD(T)/AWCVTZ level in this work, respectively. The Br−Br bond length pairs in KBr_3 were reported in 2017 to be 2.64/2.49 and 2.90/2.51 Å in *Pnma* (4 GPa) and $P\bar{3}c1$ (15 GPa) space groups, respectively.[66] These distances may be compared to our theoretical values 2.741/2.441 Å (Table 2) at the CCSD(T)/AWCVTZ level. In general, it may not be fair to compare distances in a calculated compressed crystal with our isolated molecule values at P = 1 atm.

Returning to our computational results, summarized in Table 2, in all MX_3 structures, a clear decreasing and increasing trend can be observed in the change of *B*1 (X1−X2) and *B*2 (X2−X3) bond lengths from Li to Cs, respectively. In other words, the bonds *B*1 and *B*2 tend to converge at CsX_3 with a distorted structure compared to the free X_3^- (Cl−Cl: 2.313 Å; Br−Br: 2.571 Å; I−I: 2.944 Å, Table 2), implying a decreasing interaction of M^+ with X_3^-, probably due to the increasing metal−halogen distance from Li^+ to Cs^+. Moreover, the Br_3^- and I_3^- are less distorted than Cl_3^- by the same alkali metal, in terms of the imbalance of bond pair *B*1/*B*2 in Table 2. Both *B*3 (X1−M) and *B*4 (X2−M) keep increasing because of the enlarged atomic size from Li to Cs, and the bond pair *B*3/*B*4 distances become more similar from LiX_3 to CsX_3. Particularly, the *B*3 and *B*4 distances in $CsBr_3$ and CsI_3 are almost equal with a $\Delta(B3 - B4)$ of only about 0.03−0.04 Å, whereas it is relatively large for $CsCl_3$ (~0.17 Å).

We already mentioned the $MX{\cdot}X_2$ perspective, which emerges in the next section; the similarity of *B*2 and *B*3 distances brings to mind still another viewpoint, an organometallic one: it suggests an M^+ ion π-bonding to just one pair of atoms in a trihalide anion.

Most importantly, the internuclear distance between M and atom X3 (Figure 3) is always long (mostly beyond 4.0 Å, with the exception of Li−Cl3 being 3.901 Å). Hence, no strong interaction between the alkali metal and this particular halogen atom X3 is seen. This is consistent with the observation that the MX_3 (M = Li, Na, K, Rb, Cs and X = Cl, Br, I) species all possess an asymmetric T-shaped C_s equilibrium structure, instead of a symmetric C_{2v} structure (Figure 1), which is seen for most MF_3 species.[29−31] Such a different preference of symmetry between MF_3 and MX_3 is largely dictated by the

DOI: 10.1021/acs.jpcb.7b10005
J. Phys. Chem. B 2018, 122, 3339−3353

Table 3. Harmonic Vibrational Frequencies (cm^{-1}) and Infrared Intensities (in Parentheses, km mol^{-1}) for the Isolated X_3^- (X = Cl, Br, and I) Anions Computed Using the CCSD(T)/AWCVTZ Method

	Cl_3^-		Br_3^-		I_3^-	
mode	ω^a	ω^b	ω^a	ω^b	ω^a	ω^b
ω_1 (asym stretch, σ_u)	253 (623)[c]	254	187 (250)	186	138 (151)	139
ω_2 (sym stretch, σ_g)	264 (0)[c]	261	164 (0)	161	114 (0)	112
ω_3 (bend, π_u)	161 (1)	159	89 (0)	88	57 (0)	57

[a]Harmonic vibrational frequencies in this work. [b]Harmonic vibrational frequencies reported by Dixon and co-workers (ref 5). [c]Vibrational modes for ω_1 and ω_2 switch for Cl_3^-.

Table 4. Harmonic Vibrational Frequencies (cm^{-1}) and Infrared Intensities (in Parentheses, km mol^{-1}) of the Chloride MCl_3 (M = Li, Na, K, Rb, and Cs) Molecules Predicted Using the CCSD(T)/AWCVTZ Method

	$LiCl_3$		$NaCl_3$		KCl_3		$RbCl_3$		$CsCl_3$	
	ω	expt[a]	ω	expt[a]	ω	expt[a]	ω	expt[a]	ω	expt[a]
ν_1 $(a')^b$	453 (93)	410	414 (188)	375	370 (242)	345	360 (245)	340	354 (239)	327
ν_2 $(a')^b$	576 (107)		322 (41)	276	248 (57)	258	222 (80)	223	216 (89)	225
ν_3 $(a')^b$	281 (84)		183 (25)		190 (16)		179 (10)		174 (27)	
ν_4 $(a')^b$	92 (77)		117 (113)		138 (158)		134 (140)		127 (116)	
ν_5 $(a')^b$	124 (5)		85 (8)		66 (2)		52 (1)		44 (1)	
ν_6 $(a'')^b$	108 (7)		123 (1)		138 (1)		141 (1)		143 (1)	

[a]Raman and IR fundamentals reported in the Ault and Andrews argon matrix study (ref 3). [b]The ν_{1-6} correspond to the modes 1−6 in Figure 5, respectively.

Table 5. Harmonic Vibrational Frequencies (cm^{-1}) and Infrared Intensities (in Parentheses, km mol^{-1}) of the Bromide MBr_3 (M = Li, Na, K, Rb, and Cs) Molecules Predicted Using the CCSD(T)/AWCVTZ Method[a]

	$LiBr_3$	$NaBr_3$	KBr_3	$RbBr_3$	$CsBr_3$
ν_1 $(a')^b$	244 (72)	227 (81)	225 (134), [214[c]]	220 (137)	217 (138), [206[d]/210[e]/213[f]]
ν_2 $(a')^b$	475 (88)	258 (67)	183 (23)	155 (32)	152 (40), [140[d]/136[e]/138[f]]
ν_3 $(a')^b$	283 (79)	150 (26)	141 (38)	128 (14)	122 (4)
ν_4 $(a')^b$	104 (38)	108 (47)	113 (31)	106 (30)	96 (27), [82[f]]
ν_5 $(a')^b$	76 (17)	66 (6)	50 (3)	37 (2)	29 (1)
ν_6 $(a'')^b$	77 (6)	79 (1)	82 (0)	83 (0)	84 (0)

[a]The KBr_3 and $CsBr_3$ frequencies in brackets are from experiments. [b]The ν_{1-6} correspond to the modes 1−6 in Figure 5, respectively. [c]Raman and IR frequencies reported in ref 3. [d]Raman and IR frequencies reported in refs 6, 7. [e]IR frequencies reported in ref 81. [f]Raman frequencies reported in ref 16.

Table 6. Harmonic Vibrational Frequencies (cm^{-1}) and Infrared Intensities (in Parentheses, km mol^{-1}) of the Iodide MI_3 (M = Li, Na, K, Rb, and Cs) Molecules Predicted Using the CCSD(T)/AWCVTZ Method[a]

	LiI_3	NaI_3	KI_3	RbI_3	CsI_3
ν_1 $(a')^b$	171 (56)	164 (69)	168 (67)	160 (87)	157 (88), [145[c]/145[d]/149[e]]
ν_2 $(a')^b$	417 (79)	222 (37)	149 (40)	118 (12)	110 (17), [101[c]/100[d]/103[e]/113[f]]
ν_3 $(a')^b$	273 (58)	130 (16)	106 (23)	96 (22)	90 (11)
ν_4 $(a')^b$	80 (26)	83 (27)	86 (16)	79 (10)	74 (12), [66[d]/69[e]]
ν_5 $(a')^b$	51 (7)	47 (4)	39 (4)	30 (2)	24 (1)
ν_6 $(a'')^b$	53 (8)	51 (1)	53 (0)	53 (0)	54 (0)

[a]The CsI_3 frequencies in brackets are from experiments. [b]The ν_{1-6} correspond to the modes 1−6 in Figure 5, respectively. [c]Raman and IR frequencies reported in refs 6, 7. [d]IR frequencies reported in ref 81. [e]IR frequencies reported in ref 82. [f]Raman fundamental (in solid argon) reported in ref 4.

different electronic structures of the two, which has been discussed in Introduction (see also Scheme 1).

For the angle A(X1−X2−X3) in Table 2, an ca. 6−10° deviation from linear X_3^- is noted for all MX_3 series. The LiX_3 always possess the most bent A(X1−X2−X3) angle, which is about 10° from linearity and distinct from that of NaX_3 by 3−5°. The A(X1−X2−X3) angles from NaX_3 to CsX_3 are more consistent, especially for the MCl_3. However, a slightly decreasing trend from Na to Cs can be found for the MBr_3 and MI_3 series. In the Svensson and Kloo review of triiodide structures, their Figure 10 shows small departures from triiodide linearity in hundreds of such structures. Departures from linearity of ca. 6−10° are rare, indicating in yet another way the strong M−X_3 bonding. In discrete molecules, in addition, the angle A(X1−M−X2) becomes increasingly acute due to the enlarged atomic size from Li to Cs.

In summary, our geometrical parameters show reasonable agreement with available experiments. For all three MX_3 series, the trend in geometrical change indicates a generally decreasing distortion of the X_3^- structure by M^+ from Li^+ to Cs^+. C_s (and

DOI: 10.1021/acs.jpcb.7b10005
J. Phys. Chem. B 2018, 122, 3339−3353

not C_{2v}) symmetry is established for all MX_3 (X = Cl, Br, and I). Such preference for C_s symmetry is also reflected in the MX_3 harmonic vibrational modes and frequencies, which are discussed in the following section.

Vibrational Modes and Frequencies of MX_3. Generally, for the free $D_{\infty h}$ X_3^- (X = Cl, Br, and I) anions, the antisymmetric stretch (σ_u) and bend mode (π_u) are both IR-active, whereas the symmetric stretch (σ_g) is Raman-active, as shown at the top of Figure 5. Because the MX_3 experiments necessarily contain countercations, which distort the X_3^- into a lower symmetry, both stretches are expected to have substantial intensity in the IR and Raman spectra.

In Table 3, the harmonic vibrational frequencies of the isolated X_3^- computed in this work agree to within 3 cm^{-1} of those reported by Dixon and co-workers.[5] However, with respect to the experimental MCl_3 frequencies (see Table 4) of Ault and Andrews,[3] we only observed reasonable agreement with the 258 cm^{-1} band for KCl_3. In fact, the experimental frequencies of the two prospective MCl_3 bands range from 327 to 410 cm^{-1} and 225 to 276 cm^{-1}, respectively.[3] A similar range is also noted for our computed MCl_3 frequencies. It is unclear why the two stretch frequencies of Cl_3^- vary so greatly over the range of alkali-metal countercations. The extended ranges for the computed MBr_3 and MI_3 frequencies (Tables 5 and 6) imply a similar ambiguity. This calls into question whether the two observed MX_3 bands truly correspond to the symmetric and antisymmetric stretches of X_3^-. Rather, the bonding in MX_3 establishes alternate normal modes of vibration that include substantial displacement of both the halide and metal. Therefore, a direct comparison of the frequencies of X_3^- and MX_3 is not straightforward and explicit inclusion of the alkali-metal cation is necessary.

A Complex of MX with X_2? The idea that the alkali-metal trihalides might be viewed (that's all, just a suggestion of an alternative perspective) as strongly bound complexes of MX and X_2 came from examining the detailed nature of the fundamental vibrations of these molecules.

As depicted in Figure 5, the antisymmetric and symmetric stretches of X_3^- proposed in the previous experimental study[3] of MX_3 are not found among our computed vibrational modes of MX_3. We note that the modes illustrated in Figure 5 are similar in all MX_3 (M = Li, Na, K, Rb, Cs; X = Cl, Br, I) molecules. However, for the species with heavy metals (Rb and Cs) which show relatively mild perturbation to X_3^- (judging from its distance asymmetry in Table 2), mode 2 (M−X1 stretch) is coupled with the adjacent X1−X2 stretch. Still, no sign of any well-preserved symmetric or antisymmetric stretches of the free X_3^- anion can be found from the modes of MX_3.

Figure 5 illustrates the vibrational modes for KCl_3. The fundamental vibrations of other MX_3 molecules are remarkably similar, despite the difference in internal asymmetry of the X_3 unit and distance of M from X_3. There are differences, which may be seen by comparing KCl_3 and MX_3, illustrated in SI. We also found useful a total energy distribution analysis of the vibrations, which allows one to see the internal coordinates entering a given vibration. These are tabulated in the SI (Table S2). A file allowing animation of all vibrations is available from the authors.

Only modes 1 and 6 involve displacement of the halides alone, whereas modes 2, 3, 4, and 5 involve significant displacements of the metal as well. We note that mode 1 is almost a pure X−X bond stretch; however, the stretch appears localized to a single X−X bond (X2−X3, *B*2 in Figure 3), unlike the stretches of X_3^-, which displace two X−X bonds. This is not unexpected; the equilibrium geometries of the X_3^- unit in MX_3 are unsymmetrical in just this direction. Mode 2 appears to be a localized M−X (M and X1, *B*3 in Figure 3) bond stretch. This localization of two fundamental modes of vibration, conserved across the series studied, suggests that the MX_3 system may be alternatively described as an $MX-X_2$ complex, rather than an $M^+X_3^-$ ion pair. On this basis, modes 1 and 2 should be distorted X−X and M−X stretches. Specifically, compared to the free X_2 and MX frequencies (Table 1), the localized X−X and M−X stretch frequencies of the MX_3 species (Tables 4−6) are mostly found to be lowered, and a consistently decreasing trend may be found moving from Li to Cs.

We note in passing that the optimized bond distances also show a sign of $MX-X_2$ bonding: the X1−X2 distance is always longer than X2−X3, and M−X1 is shorter than M−X2. Agreed, the differences are not large, but the trend is consistent.

While we question the previous description of the MX_3 normal modes, the corresponding frequencies computed here should still align with the experimental vibrational bands. This is because all of the modes belong to irreducible representations of the C_s point group and are thus both IR/Raman-active. So, a detailed comparison with matrix isolation experiment is in order.

As shown in Tables 3 and 4, a direct comparison of the MCl_3 harmonic vibrational frequencies with the experimental values of Ault and Andrews[3] yields generally better agreement than the previous comparison using Cl_3^-, isolated, noninteracting vibrational modes. To facilitate the assignment of the experimental bands, we note that only a few modes have the intensity necessary for detection. In addition, the noted IR spectrophotometer limit (200 cm^{-1}) of the experiment[3] precludes the observation of ν_4−ν_6 for $LiCl_3$ and ν_3−ν_6 for MCl_3 (M = Na, K, Rb, and Cs). Therefore, only ν_1 and ν_2 are candidates for assignment to the experimental IR/Raman bands.

The harmonic vibrational frequencies corresponding to ν_1 and ν_2 of the MCl_3 molecules are relatively close to the experimental values. However, there remain significant discrepancies. Deviations above 40 cm^{-1} from fundamentals are noted for ν_1 and ν_2 of $LiCl_3$ and $NaCl_3$. The ν_2 harmonic vibrational frequencies for KCl_3, $RbCl_3$, and $CsCl_3$ deviate by 20−27 cm^{-1}, which is more reasonable, but still larger than expected. For the frequencies of this magnitude, we do not expect substantially large enough anharmonic contributions to correct these deviations. A plausible reason for such deviations is that the large red shift (about 20−60 cm^{-1}, see Table S1 in the SI) noted for MX vibrational fundamentals in argon matrices[8] carries over to the MX_3 species. We recall that in Ault and Andrews's experiment,[3] MCl_3 was generated through the reaction of MCl and Cl_2 in an argon matrix at 15 K. As such, the MCl stretch was measured prior to MCl_3 formation. This stretch frequency aligns with the value reported by Jacox (see Table S1 in the SI),[8,80] confirming a similar argon-induced shift for the Ault and Andrews MCl band. By extension, their reported MCl_3 bands may be significantly shifted as well. Accordingly, assessing the agreement between gas-phase theoretical frequencies and argon matrix experimental frequencies[3] is challenging. Depending on the metal involved, ν_1 and ν_2 can be tentatively assigned to the Cl−Cl and M−Cl

DOI: 10.1021/acs.jpcb.7b10005
J. Phys. Chem. B 2018, 122, 3339−3353

Table 7. Natural Bond Orders and Natural Charges for MX_3[a]

	natural bond order: total (covalent/ionic)				natural charge			
	X1−X2 (*B*1)	X2−X3 (*B*2)	X1−M (*B*3)	X2−M (*B*4)	X1	X2	X3	M
Cl_3^-	0.50 (0.25/0.25)	0.50 (0.25/0.25)			−0.48	−0.03	−0.48	
$LiCl_3$	0.06 (0.00/0.06)	0.90 (0.82/0.08)	0.50 (0.02/0.48)	0.43 (0.01/0.42)	−0.88	0.00	−0.05	0.93
$NaCl_3$	0.08 (0.01/0.07)	0.86 (0.73/0.13)	0.89 (0.02/0.87)	0.01 (0.00/0.01)	−0.86	0.01	−0.11	0.96
KCl_3	0.13 (0.03/0.10)	0.79 (0.61/0.18)	0.75 (0.01/0.74)	0.06 (0.00/0.06)	−0.81	0.01	−0.18	0.97
$RbCl_3$	0.15 (0.04/0.11)	0.77 (0.57/0.20)	0.72 (0.01/0.71)	0.06 (0.00/0.06)	−0.79	0.01	−0.20	0.98
$CsCl_3$	0.16 (0.04/0.12)	0.75 (0.54/0.21)	0.69 (0.01/0.68)	0.07 (0.00/0.07)	−0.79	0.01	−0.21	0.98
Br_3^-	0.50 (0.25/0.25)	0.50 (0.25/0.25)			−0.48	−0.03	−0.48	
$LiBr_3$	0.13 (0.03/0.10)	0.76 (0.62/0.14)	0.47 (0.02/0.45)	0.43 (0.01/0.42)	−0.77	−0.01	−0.14	0.92
$NaBr_3$	0.15 (0.04/0.11)	0.75 (0.56/0.19)	0.74 (0.02/0.72)	0.06 (0.00/0.06)	−0.76	0.00	−0.20	0.96
KBr_3	0.30 (0.11/0.18)	0.56 (0.25/0.31)	0.25 (0.00/0.25)	0.19 (0.00/0.19)	−0.71	0.00	−0.26	0.97
$RbBr_3$	0.31 (0.12/0.19)	0.55 (0.24/0.31)	0.23 (0.00/0.23)	0.20 (0.00/0.20)	−0.70	0.01	−0.28	0.97
$CsBr_3$	0.32 (0.13/0.19)	0.54 (0.23/0.31)	0.23 (0.00/0.23)	0.20 (0.00/0.20)	−0.68	0.01	−0.30	0.98
I_3^-	0.50 (0.25/0.25)	0.50 (0.25/0.25)			−0.49	−0.03	−0.49	
LiI_3	0.15 (0.03/0.12)	0.77 (0.60/0.17)	0.53 (0.03/0.50)	0.32 (0.01/0.31)	−0.73	−0.01	−0.16	0.89
NaI_3	0.17 (0.05/0.12)	0.74 (0.54/0.20)	0.58 (0.02/0.56)	0.26 (0.00/0.26)	−0.72	−0.01	−0.21	0.94
KI_3	0.31 (0.12/0.19)	0.55 (0.25/0.30)	0.44 (0.01/0.43)	0.10 (0.00/0.10)	−0.69	0.00	−0.27	0.96
RbI_3	0.32 (0.13/0.19)	0.54 (0.24/0.30)	0.24 (0.00/0.24)	0.21 (0.00/0.21)	−0.68	0.00	−0.29	0.97
CsI_3	0.33 (0.14/0.19)	0.53 (0.23/0.30)	0.24 (0.00/0.24)	0.21 (0.00/0.21)	−0.67	0.00	−0.31	0.97

[a]The CCSD(T)/AWCVTZ geometries are used. See Figure 3 for atomic label and bond definition for MX_3.

stretches, which are probably the actual vibrational bands observed in the Ault and Andrews experiment.[3]

In comparison, there are fewer experimental results for the MBr_3 (Table 5) and MI_3 (Table 6) species. The 214 cm^{-1} KBr_3 band reported by Ault and Andrews[3] is close to our computed frequency for the localized Br−Br stretch mode (ν_1 = 225 cm^{-1}). Because the largest vibrational frequency of the free Br_3^- is predicted to be 187 cm^{-1} (Table 3), it is not reasonable to assign this 214 cm^{-1} band to Br_3^- in KBr_3. A good agreement between theory and experiments[6,7,16,81] is achieved for the $CsBr_3$ vibrational frequencies. The ν_1, ν_2, and ν_4 frequencies are computed to be 217, 152, and 96 cm^{-1}, respectively, each of which matches the observed vibrational bands within 10 cm^{-1}. Comparison of the computed frequencies of $CsBr_3$ (Table 5) and the free Br_3^- (Table 3) indicates that the 152 and 96 cm^{-1} experimental bands seemingly match those of Br_3^-, whereas the 217 cm^{-1} band does not.

For CsI_3, we find that the three vibrational frequencies from experiments[6,7,81,82] align well with our predicted harmonic values for ν_1, ν_2, and ν_4. It should be noted that each of the three computed frequencies of free I_3^- (Table 3) are in relatively good agreement with the corresponding experimental values for ν_1, ν_2, and ν_4 of CsI_3 (Table 6). This is the only case where X_3^- completely corresponds with MX_3. However, CsI_3 is an extreme case, for which the frequencies (and the geometry) tend to suggest a $Cs^+I_3^-$ ion pair, in spite of its underlying electronic structure (see next section). More generally, the experimental frequencies of $CsBr_3$ and CsI_3 were obtained from the solid state,[6,7,16,81,82] which might involve alternate electronic structures that make a direct comparison between theory and experiment ambiguous. The seemingly aligned I_3^- and CsI_3 frequencies are outliers. They by no means guarantee overall agreement across all MBr_3 and MI_3 (M = Li, Na, K, Rb, and Cs) species.

To summarize, with limited experimental data, no solid conclusion can be drawn here from the experimentally observed vibrations about whether the MBr_3 and MI_3 should be viewed more as an $M^+X_3^-$ ion pair or the $MX{-}X_2$ complex. These concerns notwithstanding, explicit consideration of the metal is instrumental in understanding the vibrational frequencies of the MX_3 species. And an $MX{-}X_2$ complex viewpoint of the bonding in the molecule, a perspective that has hitherto not received much attention, is naturally suggested by the vibrational modes. Key factors driving the vibrational frequencies are clearly evinced by an intimate examination of the electronic structure through bonding analyses.

Bonding Analyses of MX_3. Bond strength has been described theoretically in the literature by a plethora of bonding indices. Just the fact that there are so many is evidence that bond indices, even as they are carefully defined, are to some degree arbitrary. We chose to follow here the insight obtained from a natural bond orbital bond order, as defined by Weinhold and Landis.[83] The natural bond orbital (NBO) results in Table 7 show that the bond order of *B*1 (X1−X2) is consistently lower than that of *B*2 (X2−X3) for each MX_3 species. No surprise, as this follows the calculated equilibrium distances. A considerable increase of X1−X2 bond order indicates that the X1−X2 and X2−X3 become more balanced for KBr_3, $RbBr_3$, $CsBr_3$, KI_3, RbI_3, and CsI_3. For the MCl_3 species, the X2−X3 bond orders are large, approaching those of a single bond. But as the distances in Table 2 show, the corresponding bond length remains substantially longer than in Cl_2.

In the NBO formalism, it is possible to assign covalent and ionic characters to bonds.[59−61] The covalency of the X2−X3 bond is also supported by its natural bond order, comprised primarily of covalent contributions (Table 7), although an increasing ionic character of the X2−X3 bond can be found on moving from $LiCl_3$ to $CsCl_3$. The preference of covalent over ionic character is switched for KBr_3, $RbBr_3$, $CsBr_3$, KI_3, RbI_3, and CsI_3, in which the X2−X3 bonds possess slightly more ionic features than covalency. This is in accordance with the increased negative charges on atom X3, as shown in Table 7.

The calculated charge distribution shows almost complete electron transfer from the metal ion to the trihalide. And in the

DOI: 10.1021/acs.jpcb.7b10005
J. Phys. Chem. B 2018, 122, 3339−3353

trihalide, no matter how asymmetric it is, the net charge on the central atom, X1 is close to zero. The electron transferred is distributed, in an asymmetric fashion consistent with the asymmetry of the bonding, among X1 and X3. The pileup of electron density at the termini of a three-center electron-rich system is what one would expect; it is connected, in another context, to the presence of strongly electronegative fluorides at the termini and not the middle of such bonds (e.g., FXeF).

The presence of the metal cation engenders localization of electron density mostly onto X1, as shown by the natural charges in Table 7. Orbital interactions based on the NBO perturbation theory analysis (see Theoretical Methods) shows that the leading interaction between the X1 and X2−X3 units is always the donation of an X1 lone pair n(X1) into the X2−X3 antibonding orbital σ^*(X2−X3) for all MX_3 species. Thus, strengthened X1−X2 and weakened X2−X3 bonds are expected. The energies for this $n(X1) \rightarrow \sigma^*(X2-X3)$ interaction (see SI) gradually increase from LiX_3 to CsX_3 (X = Cl, Br, or I). Therefore, the bond orders of X1−X2 and X2−X3 are expected to increase and decrease, respectively. This finding aligns with the trends for the natural bond orders of X1−X2 and X2−X3 given in Table 7. Also, this is consistent with the decreasing X1−X2 and increasing X2−X3 bond lengths in Table 2.

The general picture that emerges is consistent with the donor−acceptor picture of bonding in the trihalide anions, at one end of a bonding spectrum, symmetrical electron-rich bonding at the other end.[20−24]

Both $B3$ (X1−M) and $B4$ (X2−M) bonds possess some "purely" ionic character, supported by the natural charges and their predominant ionic bond orders reported in Table 7. For the MCl_3 series, except for the similar X1−M and X2−M bond orders for $LiCl_3$, the X1−M bond orders for the other species are much higher than the X2−M bond orders, but comparable to the corresponding X2−X3 ($B2$) covalent bonds. This observation supports a view of MCl_3 as formed from MX and X_2 interacting through weaker X1−X2 and X2−M bonds. For the bromides and iodides, however, a considerably decreased X1−M bond order for KBr_3, $RbBr_3$, $CsBr_3$, KI_3, RbI_3, and CsI_3 can be noted, coupled to the generally increased X1−X2 and X2−M bond orders. This is another indication that the X_3^- is less impacted by the larger metal atoms than the smaller ones, which also leaves these species standing at a borderline between the MX−X_2 complex and the $M^+X_3^-$ ion pair. However, the featured antisymmetric and symmetric stretches of X_3^- are not clearly exhibited in their vibrational modes discussed previously.

To further correlate the NBO results with the vibrational frequencies, the gradually increasing interaction energies (see SI) for the donor−acceptor interaction $[n(X1) \rightarrow \sigma^*(X2-X3)]$ from LiX_3 to CsX_3 rationalize the increasingly shifted X−X stretch frequencies (Tables 4−6) in MX_3, relative to the frequencies of corresponding free diatomic X_2 species (Table 1). The increasing dative interaction from Li to Cs leads to a greater σ^*(X2−X3) orbital occupation, which weakens the X2−X3 bond ($B2$) and therefore lowers the X−X stretch frequencies. On the other hand, a comparison of the M−X stretch frequencies of MX_3 and the free MX shows that the X1−M ($B3$) stretch in MX_3 becomes decreasingly impacted from Li to Cs. The physical origins of this trend seem ambiguous. One possible explanation is that its displacement of the metal in the M−X1 stretch decreases as it becomes heavier, making any perturbation from the X_2 moiety have less impact.

QTAIM. All of the molecules studied feature bond critical points for every short contact. This is shown in Figure 6 for a typical molecule, KCl_3.

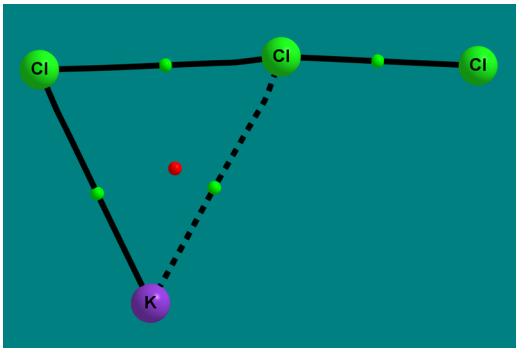

Figure 6. Bader analysis for the C_s MX_3 (illustrated for KCl_3), including bond critical points (BCPs, green) and ring critical point (RCP, red). The dashed line for the central KCl bond indicates a CP density below the "weak CP threshold" of 0.025 a.u.

Our results from Bader's quantum theory of atoms in molecules (QTAIM) are reported in detail in the SI. Consistent with above NBO results (Table 7), the electron density at the bond critical points (BCPs) of $B1$ (X1−X2) is lower than that of $B2$ (X2−X3) for each MX_3 species, suggesting a consistently stronger X2−X3 bond than the X1−X2 bond. Similar to the NBO results from LiX_3 to CsX_3, the trends in BCP densities of the X1−X2 bonds (increasing) and X2−X3 bonds (decreasing) indicate that the two bonds become more balanced. In Bader's characterization of atomic interactions,[84] the Laplacian of the electron densities $\nabla^2\rho$(BCP) in Table S3 (in the SI) should provide general bonding features of the MX_3 systems. The consistently smaller $\nabla^2\rho$(BCP) of the X2−X3 bond compared to the X1−X2 bond implies that the former possesses more covalency than the latter. In addition, the X2−X3 $\nabla^2\rho$(BCP) increases from LiX_3 to CsX_3, suggesting an increasing ionic and decreasing covalent character.

In summary, the bonding trends explored with NBO and QTAIM approaches clearly show that X1−X2 and X2−X3 become more balanced from LiX_3 to CsX_3, although they are never as "truly" balanced as in the free $D_{\infty h}$ symmetric X_3^-. We are led to the same conclusion drawn from the structures (Table 2) of MX_3: a decreasing effect of the M^+ cation on the X_3^- anions from LiX_3 to CsX_3. A comparison of the bonding types of X_3^- (Scheme 1) and MX_3 (Table 7) shows that the two equal contributors (bonding types I and II) to the bonding in X_3^- anions collapse into mostly just one of the two for MX_3, mainly depending on the position of the metal cations.

Thermochemistry of MX_3. The reaction energies (D_0, corrected by ZPVE) of three different dissociation pathways

$$MX_3 \rightarrow MX + X_2$$

$$MX_3 \rightarrow M^+ + X_3^-$$

$$MX_3 \rightarrow M + X_3$$

are summarized in Table 8. The reason for studying the neutral version of the $MX_3 \rightarrow M^+ + X_3^-$ fragmentation is that ionic fragmentation is naturally more endothermic than neutral ones. In all cases, the dissociation energy for the $MX_3 \rightarrow MX + X_2$ reaction is much lower than that of the $MX_3 \rightarrow M^+ + X_3^-$ (or $MX_3 \rightarrow M + X_3$) dissociation. This result supports our previous

DOI: 10.1021/acs.jpcb.7b10005
J. Phys. Chem. B 2018, 122, 3339−3353

Table 8. Endothermicities (D_0, kcal mol^{-1}) of the Three Different Dissociation Processes for MX_3 (M = Li, Na, K, Rb, and Cs; X = Cl, Br, and I) Molecules Predicted Using the B3LYP3/AVTZ Method

species	D_0 ($MX_3 \rightarrow MX + X_2$)	D_0 ($MX_3 \rightarrow M^+ + X_3^-$)	D_0 ($MX_3 \rightarrow M + X_3$)
$LiCl_3$	10.0	134.8	115.1
$NaCl_3$	11.2	114.1	99.0
KCl_3	12.9	100.3	105.6
$RbCl_3$	13.3	95.8	105.8
$CsCl_3$	13.1	91.6	108.9
$LiBr_3$	14.3	127.6	101.8
$NaBr_3$	15.3	109.1	87.9
KBr_3	17.5	95.7	95.0
$RbBr_3$	17.9	91.3	95.3
$CsBr_3$	18.0	87.3	98.6
LiI_3	15.0	120.7	88.4
NaI_3	15.2	104.0	76.3
KI_3	17.3	90.5	83.2
RbI_3	17.5	86.0	83.4
CsI_3	18.1	82.2	87.0

conclusion indicating that the MX_3 system is also well described as an MX−X_2 complex, rather than an $M^+X_3^-$ ion pair.

A note on the numbers in the last two columns: the energetics is a reflection of the differences in the ionization potentials of the metal atoms (falling from 5.5 eV for Li to 3.9 eV for Cs), and the vertical electron affinities of the neutral X_3 species. The latter are remarkably high, 4−5 eV. For the $MX_3 \rightarrow MX + X_2$ dissociation, an increasing trend for D_0 can be noted from LiX_3 to CsX_3 (X = Cl, Br, or I). This is consistent with the increasing trend for D_0 in the fluoride $MF_3 \rightarrow MF + F_2$ (M = Na, K, Rb, and Cs) series reported by Tozer and Sosa.[29] In addition, previous experiments determined the bond strengths ($X_3^- \rightarrow X_2 + X^-$) of the isolated Cl_3^-, Br_3^-, and I_3^- to be about 24, 30, and 30 kcal mol^{-1} in the gas phase, respectively.[9,10] Those values are about twice the D_0 values computed here for the $MX_3 \rightarrow MX + X_2$ dissociations. This is additional evidence that presence of an alkali-metal cation weakens the X−X covalent band of X_3^-, favoring localization of more electron density on a terminal X atom. For the $MX_3 \rightarrow M^+ + X_3^-$ dissociation, a decreasing trend in D_0 can be found from LiX_3 to CsX_3 (X = Cl, Br, or I). This indicates that the distortion of X_3^- by M^+ decreases with increasing cation size, caused by the increasing distance between M^+ and X^- as well as the decreasing M−X orbital overlap from LiX_3 to CsX_3. This agrees well with the structural trend for increasingly balanced X1−X2 and X2−X3 bond lengths (Figure 3 and Table 2) moving from LiX_3 to CsX_3.

CONCLUSIONS

The alkali-metal trihalides MX_3 (M = Li, Na, K, Rb, Cs; X = Cl, Br, I) are systematically studied here using coupled-cluster methods with the weighted core-valence correlation-consistent basis sets (new basis sets for K, Rb, and Cs). Benchmarks comparing the CCSD(T) method against experimental results show satisfactory performance for the new basis sets in predicting reliable structures and harmonic vibrational frequencies for the relevant diatomic species MX and X_2. An isomer search using the B3LYP functional confirms a planar asymmetric T-shaped structure as the global minimum for all MX_3 species.

The CCSD(T) computations suggest a strong distortion of the X_3^- anions by the alkali-metal countercations M^+, in the equilibrium geometries, vibrational spectra, bonding, and thermochemistry. For the vibrational modes, the well-established antisymmetric and symmetric stretches of the free X_3^- anions are not retained in any MX_3 species. Instead, localized and mutually perturbed X−X and M−X stretches are involved. For the vibrational frequencies, a comparison of our theoretical MX_3 harmonic vibrational frequencies with the experimental fundamentals yields generally better agreement than the previous comparison using the free X_3^- anions. In a bonding analysis, the NBO and QTAIM results show low natural bond orders and electron densities at the bond critical points between MX and X_2, respectively. In the thermochemistry, the $MX_3 \rightarrow MX + X_2$ dissociation pathway has a much smaller endothermicity than the $MX_3 \rightarrow M^+ + X_3^-$ (or $MX_3 \rightarrow M + X_3$) pathway. All of the above-mentioned results lead us to suggest that the MX_3 system might alternatively be described as an MX−X_2 complex rather than the $M^+X_3^-$ ion pair proposed in previous studies.[1−4]

Our conclusions are likely applicable only to the MX_3 systems in the gas phase, in inert matrices (argon and neon), or in nonpolar solvents if possible, as no strong solvation would be expected. Strong solvation of M^+ and X_3^- ions in polar solvents (H_2O, for instance) could make the $M^+X_3^-$ ion pair an appropriate description for the MX_3 systems. Such solvation phenomena on the molecular and electronic structures of X_3^- are known as a crucial part of understanding their electrochemistry in electrolytic media,[85,86] a subject beyond present study.

The two perspectives on MX_3 molecules, strong complexation of trihalide anions by metal cations and strong interaction of polar MX molecules with dihalogens, are complementary to each other, each with its own advantages and consequences. We hope the chemistry of these remarkable molecules will benefit from keeping both pictures of the bonding in them in view.

ASSOCIATED CONTENT

Supporting Information

The Supporting Information is available free of charge on the ACS Publications website at DOI: 10.1021/acs.jpcb.7b10005.

Convergence parameters used for programs; the cc-pwCVTZ-PP basis sets for K, Rb, and Cs; and detailed information of all species (PDF)

DOI: 10.1021/acs.jpcb.7b10005
J. Phys. Chem. B 2018, 122, 3339−3353

AUTHOR INFORMATION

Corresponding Authors

*E-mail: ccq@uga.edu (H.F.S.).
*E-mail: rh34@cornell.edu (R.H.).

ORCID

J. Grant Hill: 0000-0002-6457-5837
Kirk A. Peterson: 0000-0003-4901-3235
Henry F. Schaefer III: 0000-0003-0252-2083
Roald Hoffmann: 0000-0001-5369-6046

Notes

The authors declare no competing financial interest.

ACKNOWLEDGMENTS

This research was supported by the U.S. National Science Foundation (Grant No. CHE-1361178) and the Engineering and Physical Sciences Research Council (U.K., project EP/N02253X/1). The authors thank Professor Frank A. Weinhold (University of Wisconsin−Madison) and Dr. Yaoming Xie (CCQC, University of Georgia) for helpful discussions concerning the NBO analyses.

REFERENCES

(1) Ault, B. S.; Andrews, L. Salt-Molecule Matrix Reactions. Infrared Spectra of the $M^+HCl_2^-$ and $M^+Cl_3^-$ Ion Pairs in Solid Argon. *J. Am. Chem. Soc.* **1975**, *97*, 3824−3826.

(2) Andrews, L. Optical Spectra of the Difluoride, Dichloride, and Trichloride Ions in the Matrix-Isolated $M^+F_2^-$, $M^+Cl_2^-$, and $M^+Cl_3^-$ Species. *J. Am. Chem. Soc.* **1976**, *98*, 2147−2152.

(3) Ault, B. S.; Andrews, L. Infrared and Raman Spectra of the $M^+Cl_3^-$ Ion Pairs and Their Chlorine−Bromine Counterparts Isolated in Argon Matrices. *J. Chem. Phys.* **1976**, *64*, 4853−4859.

(4) Andrews, L.; Prochaska, E. S.; Loewenschuss, A. Resonance Raman and Ultraviolet Absorption Spectra of the Triiodide Ion Produced by Alkali Iodide-Iodine Argon Matrix Reactions. *Inorg. Chem.* **1980**, *19*, 463−465.

(5) Thanthiriwatte, K. S.; Spruell, J. M.; Dixon, D. A.; Christe, K. O.; Jenkins, H. D. B. Structures, Vibrational Frequencies, and Stabilities of Halogen Cluster Anions and Cations, $X_n^{+/-}$, n = 3, 4, and 5. *Inorg. Chem.* **2014**, *53*, 8136−8146.

(6) Gabes, W.; Gerding, H. Vibrational Spectra and Structures of the Trihalide Ions. *J. Mol. Struct.* **1972**, *14*, 267−279.

(7) Gabes, W.; Elst, R. Force Constants of the Trihalide Ions. *J. Mol. Struct.* **1974**, *21*, 1−5.

(8) Jacox, M. E. Comparison of the Ground State Vibrational Fundamentals of Diatomic Molecules in the Gas Phase and in Inert Solid Matrices. *J. Mol. Spectrosc.* **1985**, *113*, 286−301.

(9) Do, K.; Klein, T. P.; Pommerening, C. A.; Sunderlin, L. S. A New Flowing Afterglow-Guided Ion Beam Tandem Mass Spectrometer. Applications to the Thermochemistry of Polyiodide Ions. *J. Am. Soc. Mass. Spectrom.* **1997**, *8*, 688−696.

(10) Nizzi, K. E.; Pommerening, C. A.; Sunderlin, L. S. Gas-Phase Thermochemistry of Polyhalide Anions. *J. Phys. Chem. A* **1998**, *102*, 7674−7679.

(11) Person, W. B.; Anderson, G. R.; Fordemwalt, J. N.; Stammreich, H.; Forneris, R. Infrared and Raman Spectra, Force Constants, and the Structures of Some Polyhalide Ions: ICl_2^-, ICl_4^-, $BrCl_2^-$, and Br_3^-. *J. Chem. Phys.* **1961**, *35*, 908−914.

(12) Nelson, I. V.; Iwamoto, R. T. Voltammetric Evaluation of the Stability of Trichloride, Tribromide, and Triiodide Ions in Nitromethane, Acetone, and Acetonitrile. *J. Electroanal. Chem.* **1964**, *7*, 218−221.

(13) Robertson, K. N.; Cameron, T. S.; Knop, O. Polyhalide Anions in Crystals. Part 2. I_3^- Asymmetry and NH...I Bonding: Triiodides of the $Me_2NH_2^+$, Ph_2I^+, Tropanium, *N,N,N′,N′*-Me_4-1,2-ethanediammonium, *N,N,N′,N′*-Me_4-1,3-propanediammonium, *N*-Me-piperazinium(2+), and *N,N′*-Me_2-piperazinium(2+) Cations, and Me_2NH_2I. *Can. J. Chem.* **1996**, *74*, 1572−1591.

(14) Robertson, K. N.; Bakshi, P. K.; Cameron, T. S.; Knop, O. Polyhalide Anions in Crystals. 3. The Br_8^{2-} Anion in Diquinuclidinium Octabromide, the Crystal Structures of Me_4PBr_3 and Quinuclidinium Tribromide, and Ab Initio Calculations on Polybromide Anions. *Z. Anorg. Allg. Chem.* **1997**, *623*, 104−114.

(15) Evans, J. C.; Lo, G. Y.-S. Vibrational Spectra of Cl_3^- Ion and Evidence for Existence of Cl_5^-. *J. Chem. Phys.* **1966**, *44*, 3638−3639.

(16) Burns, G. R.; Renner, R. M. A Raman and Resonance Raman Study of Polybromide Anions and a Study of the Temperature Dependence of the Raman-Active Phonons of Tetrabutylaminonium Tribromide. *Spectrochim. Acta, Part A* **1991**, *47*, 991−999.

(17) Hunt, R. D.; Thompson, C.; Hassanzadeh, P.; Andrews, L. Matrix IR Spectra of the Products from Fluorine Molecule, Chlorine Molecule, and Chlorine Fluoride (ClF) Reactions with Pulsed-Laser Evaporated Uranium Atoms. *Inorg. Chem.* **1994**, *33*, 388−391.

(18) Tuinman, A. A.; Gakh, A. A.; Hinde, R. J.; Compton, R. N. The First Direct Observation of the Trifluoride Anion (F_3^-) in the Gas Phase. *J. Am. Chem. Soc.* **1999**, *121*, 8397−8398.

(19) Artau, A.; Nizzi, K. E.; Hill, B. T.; Sunderlin, L. S.; Wenthold, P. G. Bond Dissociation Energy in Trifluoride Ion. *J. Am. Chem. Soc.* **2000**, *122*, 10667−10670.

(20) Landrum, G. A.; Goldberg, N.; Hoffmann, R. Bonding in the Trihalides (X_3^-), Mixed Trihalides (X_2Y^-) and Hydrogen Bihalides (X_2H^-). The Connection between Hypervalent, Electron-Rich Three-Center, Donor-Acceptor and Strong Hydrogen Bonding. *J. Chem. Soc., Dalton Trans.* **1997**, 3605−3613.

(21) Munzarová, M. L.; Hoffmann, R. Electron-Rich Three-Center Bonding: Role of s,p Interactions across the p-Block. *J. Am. Chem. Soc.* **2002**, *124*, 4787−4795.

(22) Braïda, B.; Hiberty, P. C. What Makes the Trifluoride Anion F_3^- So Special? A Breathing-Orbital Valence Bond ab Initio Study. *J. Am. Chem. Soc.* **2004**, *126*, 14890−14898.

(23) Braïda, B.; Hiberty, P. C. Application of the Valence Bond Mixing Configuration Diagrams to Hypervalency in Trihalide Anions: A Challenge to the Rundle-Pimentel Model. *J. Phys. Chem. A* **2008**, *112*, 13045−13052.

(24) Ciancaleoni, G.; Arca, M.; Caramori, G. F.; Frenking, G.; Schneider, F. S. S.; Lippolis, V. Bonding Analysis in Homo- and Hetero-Trihalide Species: A Charge Displacement Study. *Eur. J. Inorg. Chem.* **2016**, *2016*, 3804−3812.

(25) Hach, R. J.; Rundle, R. E. The Structure of Tetramethylammonium Pentaiodide. *J. Am. Chem. Soc.* **1951**, *73*, 4321−4324.

(26) Pimentel, G. C. The Bonding of Trihalide and Bifluoride Ions by the Molecular Orbital Method. *J. Chem. Phys.* **1951**, *19*, 446−448.

(27) Heard, G. L.; Marsden, C. J.; Scuseria, G. E. The Trifluoride Anion: A Difficult Challenge for Quantum Chemistry. *J. Phys. Chem.* **1992**, *96*, 4359−4366.

(28) Mota, F.; Novoa, J. J. The Symmetry Breaking Problem in the Triflouride Anion: A Multireference Approach. *J. Chem. Phys.* **1996**, *105*, 8777−8784.

(29) Tozer, D. J.; Sosa, C. P. The Alkali Metal Trifluorides $M^+F_3^-$: How Well Can Theory Predict Experiment? *Mol. Phys.* **1997**, *90*, 515−524.

(30) Getmanskii, I. V.; Koval, V. V.; Minyaev, R. M.; Minkin, V. I. Dependence of the Structure of Alkali Metal−Trifluoride Ion Pairs $F_3^-M^+$ on the Counterion M^+ (M = Li, Na, K). *Mendeleev Commun.* **2015**, *25*, 417−419.

(31) Vent-Schmidt, T.; Brosi, F.; Metzger, J.; Schlöder, T.; Wang, X.; Andrews, L.; Müller, C.; Beckers, H.; Riedel, S. Fluorine-Rich Fluorides: New Insights into the Chemistry of Polyfluoride Anions. *Angew. Chem., Int. Ed.* **2015**, *54*, 8279−8283.

(32) Ault, B. S.; Andrews, L. Matrix Reactions of Alkali Metal Fluoride Molecules with Fluorine. Infrared and Raman Spectra of the Trifluoride Ion in the $M^+F_3^-$ Species. *J. Am. Chem. Soc.* **1976**, *98*, 1591−1593.

DOI: 10.1021/acs.jpcb.7b10005
J. Phys. Chem. B 2018, 122, 3339−3353

(33) Ault, B. S.; Andrews, L. Infrared and Raman Spectra of the $M^+F_3^-$ Ion Pairs and Their Mixed Chlorine-Fluorine Counterparts in Solid Argon. *Inorg. Chem.* **1977**, *16*, 2024−2028.
(34) Vosko, S. H.; Wilk, L.; Nusair, M. Accurate Spin-Dependent Electron Liquid Correlation Energies for Local Spin Density Calculations: A Critical Analysis. *Can. J. Phys.* **1980**, *58*, 1200−1211.
(35) Becke, A. D. Density-Functional Exchange-Energy Approximation with Correct Asymptotic Behavior. *Phys. Rev. A* **1988**, *38*, 3098−3100.
(36) Lee, C.; Yang, W.; Parr, R. G. Development of the Colle-Salvetti Correlation-Energy Formula into a Functional of the Electron-Density. *Phys. Rev. B* **1988**, *37*, 785−789.
(37) Werner, H.-J.; Knowles, P. J.; Knizia, G.; Manby, F. R.; Schütz, M. MOLPRO: A General-Purpose Quantum Chemistry Program Package. *Wiley Interdiscip. Rev.: Comput. Mol. Sci.* **2012**, *2*, 242−253.
(38) Werner, H.-J.; Knowles, P. J.; Knizia, G.; Manby, F. R.; Schütz, M.; Celani, P.; Györffy, W.; Kats, D.; Korona, T.; Lindh, R. et al. *MOLPRO*, version 2010.1, a package of ab initio programs; 2010, see http://www.molpro.net/info/2010.1/doc/quickstart/node1.html.
(39) Prascher, B. P.; Woon, D. E.; Peterson, K. A.; Dunning, T. H.; Wilson, A. K. Gaussian Basis Sets for Use in Correlated Molecular Calculations. VII. Valence, Core-Valence, and Scalar Relativistic Basis Sets for Li, Be, Na, and Mg. *Theor. Chem. Acc.* **2011**, *128*, 69−82.
(40) Hill, J. G.; Peterson, K. A. Gaussian Basis Sets for Use in Correlated Molecular Calculations. XI. Pseudopotential-based and All-electron Relativistic Basis Sets for Alkali Metal (K−Fr) and Alkaline Earth (Ca−Ra) Elements. *J. Chem. Phys.* **2017**, *147*, 244106.
(41) Woon, D. E.; Dunning, T. H. Gaussian Basis Sets for Use in Correlated Molecular Calculations. III. The Atoms Aluminum through Argon. *J. Chem. Phys.* **1993**, *98*, 1358−1371.
(42) Peterson, K. A.; Figgen, D.; Goll, E.; Stoll, H.; Dolg, M. Systematically Convergent Basis Sets with Relativistic Pseudopotentials. II. Small-Core Pseudopotentials and Correlation Consistent Basis Sets for the Post-*d* Group 16−18 Elements. *J. Chem. Phys.* **2003**, *119*, 11113−11123.
(43) Raghavachari, K.; Trucks, G. W.; Pople, J. A.; Head-Gordon, M. A Fifth-Order Perturbation Comparison of Electron Correlation Theories. *Chem. Phys. Lett.* **1989**, *157*, 479−483.
(44) Bartlett, R. J.; Watts, J. D.; Kucharski, S. A.; Noga, J. Non-Iterative Fifth-Order Triple and Quadruple Excitation Energy Corrections in Correlated Methods. *Chem. Phys. Lett.* **1990**, *165*, 513−522.
(45) Stanton, J. F. Why CCSD(T) Works: A Different Perspective. *Chem. Phys. Lett.* **1997**, *281*, 130−134.
(46) Shavitt, I.; Bartlett, R. J. *Many-Body Methods in Chemistry and Physics: MBPT and Coupled-Cluster Theory*; Cambridge University Press: Cambridge, U.K., 2009.
(47) Harding, M. E.; Metzroth, T.; Gauss, J.; Auer, A. A. Parallel Calculation of CCSD and CCSD(T) Analytic First and Second Derivatives. *J. Chem. Theory Comput.* **2008**, *4*, 64−74.
(48) CFOUR, a quantum chemical program package by Stanton, J. F.; Gauss, J.; Harding, M. E.; Szalay, P. G. with contributions from Auer, A. A.; Bartlett, R. J.; Benedikt, U.; Berger, C.; Bernholdt, D. E.; Bomble, Y. J.; Cheng, L.; Christiansen, O.; Heckert, M.; Heun, O. et al., and the integral packages *MOLECULE* (Almlöf, J.; Taylor, P. R.), *PROPS* (Taylor, P. R.), *ABACUS* (Helgaker, T.; Jensen, H. J. Aa.; Jørgensen, P.; Olsen, J.), and ECP routines by Mitin, A. V.; van Wüllen, C. For the current version see, http://www.cfour.de.
(49) Peterson, K. A.; Dunning, T. H. Accurate Correlation Consistent Basis Sets for Molecular Core−Valence Correlation Effects: The Second Row Atoms Al−Ar, and the First Row Atoms B−Ne Revisited. *J. Chem. Phys.* **2002**, *117*, 10548−10560.
(50) Peterson, K. A.; Shepler, B. C.; Figgen, D.; Stoll, H. On the Spectroscopic and Thermochemical Properties of ClO, BrO, IO, and Their Anions. *J. Phys. Chem. A* **2006**, *110*, 13877−13883.
(51) Peterson, K. A.; Yousaf, K. E. Molecular Core-Valence Correlation Effects Involving the Post-D Elements Ga−Rn: Benchmarks and New Pseudopotential-Based Correlation Consistent Basis Sets. *J. Chem. Phys.* **2010**, *133*, No. 174116.
(52) Lim, I. S.; Schwerdtfeger, P.; Metz, B.; Stoll, H. All-Electron and Relativistic Pseudopotential Studies for the Group 1 Element Polarizabilities from K to Element 119. *J. Chem. Phys.* **2005**, *122*, No. 104103.
(53) Blaudeau, J. P.; Brozell, S. R.; Matsika, S.; Zhang, Z.; Pitzer, R. M. Atomic Orbital Basis Sets for Use with Effective Core Potentials. *Int. J. Quantum Chem.* **2000**, *77*, 516−520.
(54) Christiansen, P. A. Basis Sets in Correlated Effective Potential Calculations. *J. Chem. Phys.* **2000**, *112*, 10070−10074.
(55) Peterson, K. A. Systematically Convergent Basis Sets with Relativistic Pseudopotentials. I. Correlation Consistent Basis Sets for the Post-*d* Group 13−15 Elements. *J. Chem. Phys.* **2003**, *119*, 11099−11112.
(56) Glendening, E. D.; Landis, C. R.; Weinhold, F. Natural Bond Orbital Methods. *Wiley Interdiscip. Rev.: Comput. Mol. Sci.* **2012**, *2*, 1−42.
(57) Matta, C. F.; Boyd, R. J. *The Quantum Theory of Atoms in Molecules*; Wiley-VCH Verlag GmbH & Co. KGaA, 2007; pp 1−34.
(58) Glendening, E. D.; Badenhoop, J. K.; Reed, A. E.; Carpenter, J. E.; Bohmann, J. A.; Morales, C. M.; Landis, C. R.; Weinhold, F. *NBO 6.0.*; Theoretical Chemistry Institute, University of Wisconsin: Madison, 2013.
(59) Glendening, E. D.; Badenhoop, J. K.; Weinhold, F. Natural Resonance Theory: III. Chemical Applications. *J. Comput. Chem.* **1998**, *19*, 628−646.
(60) Glendening, E. D.; Weinhold, F. Natural Resonance Theory: I. General Formalism. *J. Comput. Chem.* **1998**, *19*, 593−609.
(61) Glendening, E. D.; Weinhold, F. Natural Resonance Theory: II. Natural Bond Order and Valency. *J. Comput. Chem.* **1998**, *19*, 610−627.
(62) Keith, T. A. *AIMAll*, version 16.01.09; TK Gristmill Software: Overland Park, KS, 2016.
(63) *NIST Chemistry WebBook, NIST Standard Reference Database Number 69*; Linstrom, P. J., Mallard, W. G., Eds.; National Institute of Standards and Technology: Gaithersburg MD, http://webbook.nist.gov/cgi/cbook.cgi?Contrib=.
(64) Brückner, R.; Haller, H.; Ellwanger, M.; Riedel, S. Polychloride Monoanions from $[Cl_3]^-$ to $[Cl_9]^-$: A Raman Spectroscopic and Quantum Chemical Investigation. *Chem. − Eur. J.* **2012**, *18*, 5741−−5747.
(65) Pichierri, F. Structure and Bonding in Polybromide Anions $Br^-(Br_2)_n$ (n = 1−6). *Chem. Phys. Lett.* **2011**, *515*, 116−121.
(66) Patel, N. N.; Verma, A. K.; Mishra, A. K.; Sunder, M.; Sharma, S. M. The Synthesis of Unconventional Stoichiometric Compounds in the K-Br System at High Pressures. *Phys. Chem. Chem. Phys.* **2017**, *19*, 7996−8007.
(67) Breneman, G. L.; Willett, R. D. The Crystal Structure of Cesium Tribromide and a Comparison of the Br_3^- and I_3^- Systems. *Acta Crystallogr., Sect. B: Struct. Crystallogr. Cryst. Chem.* **1969**, *25*, 1073−1076.
(68) Tebbe, K. F.; Georgy, U. The Crystal-Structures of Rubidium Triiodide and Thallium Triiodide. *Acta Crystallogr., Sect. C: Cryst. Struct. Commun.* **1986**, *42*, 1675−1678.
(69) Tasman, H. A.; Boswijk, K. H. CORRECTION. *Acta Crystallogr.* **1955**, *8*, 857.
(70) Tasman, H. A.; Boswijk, K. H. Re-Investigation of the Crystal Structure of CsI_3. *Acta Crystallogr.* **1955**, *8*, 59−60.
(71) Groom, C. R.; Bruno, I. J.; Lightfoot, M. P.; Ward, S. C. The Cambridge Structural Database. *Acta Crystallogr., Sect. B: Struct. Sci.* **2016**, *72*, 171−179.
(72) Svensson, P. H.; Kloo, L. Synthesis, Structure, and Bonding in Polyiodide and Metal Iodide−Iodine Systems. *Chem. Rev.* **2003**, *103*, 1649−1684.
(73) Runsink, J.; Swen-Walstra, S.; Migchelsen, T. Refinement of the Crystal Structures of $(C_6H_5)_4AsI_3$ and CsI_3 at 20 °C and at −160 °C. *Acta Crystallogr., Sect. B: Struct. Crystallogr. Cryst. Chem.* **1972**, *28*, 1331−1335.

DOI: 10.1021/acs.jpcb.7b10005
J. Phys. Chem. B 2018, 122, 3339−3353

(74) Rogachev, A. Yu.; Hoffmann, R. Hypervalent Compounds as Ligands: I_3-Anion Adducts with Transition Metal Pentacarbonyls. *Inorg. Chem.* **2013**, *52* (12), 7161−7171.
(75) Wei, S.; Wang, J.; Deng, S.; Zhang, S.; Li, Q. Hypervalent Iodine with Linear Chain at High Pressure. *Sci. Rep.* **2015**, *5*, No. 14393.
(76) Havinga, E. E.; Boswijk, K. H.; Wiebenga, E. H. The Crystal Structure of Cs_2I_8 (CsI_4). *Acta Crystallogr.* **1954**, *7*, 487−490.
(77) Toman, K.; Honzl, J.; Jecny, J. The Crystal Structure of a Polyiodide Complex with *N*-methylacetamide - $KI.KI_3.6$-($CH_3CONHCH_3$). *Acta Crystallogr.* **1965**, *18*, 673−677.
(78) Thomas, R.; Moore, F. H. Neutron Diffraction Studies of Polyiodides. I. Potassium Triiodide Monohydrate. *Acta Crystallogr., Sect. B: Struct. Crystallogr. Cryst. Chem.* **1980**, *36*, 2869−2873.
(79) Zhang, W.; Oganov, A. R.; Goncharov, A. F.; Zhu, Q.; Boulfelfel, S. E.; Lyakhov, A. O.; Stavrou, E.; Somayazulu, M.; Prakapenka, V. B.; Konôpková, Z. Unexpected Stable Stoichiometries of Sodium Chlorides. *Science* **2013**, *342*, 1502−1505.
(80) Jacox, M. E. The Spectroscopy of Molecular Reaction Intermediates Trapped in the Solid Rare Gases. *Chem. Soc. Rev.* **2002**, *31*, 108−115.
(81) Vincent, H.; Monteil, Y.; Berthet, M. P. The Thiotrithiazyl Iodated Polyhalides. *J. Inorg. Nucl. Chem.* **1980**, *42*, 5−7.
(82) Maki, A. G.; Forneris, R. Infrared and Spectra of Some Trihalide Ions: ICl_2^-, IBr_2^-, I_3^-, I_2Br^-, and $BrICl^-$. *Spectrochim. Acta, Part A* **1967**, *23*, 867−880.
(83) Weinhold, F.; Landis, C. R. *Valency and Bonding: A Natural Bond Orbital Donor-Acceptor Perspective*; Cambridge University Press, 2005.
(84) Bader, R. F. W.; Essén, H. The Characterization of Atomic Interactions. *J. Chem. Phys.* **1984**, *80*, 1943−1960.
(85) Eriksson, S. K.; Josefsson, I.; Ottosson, N.; Öhrwall, G.; Björneholm, O.; Siegbahn, H.; Hagfeldt, A.; Odelius, M.; Rensmo, H. Solvent Dependence of the Electronic Structure of I^- and I_3^-. *J. Phys. Chem. B* **2014**, *118*, 3164−3174.
(86) Jena, N. K.; Josefsson, I.; Eriksson, S. K.; Hagfeldt, A.; Siegbahn, H.; Björneholm, O.; Rensmo, H.; Odelius, M. Solvent-Dependent Structure of the I_3^- Ion Derived from Photoelectron Spectroscopy and Ab Initio Molecular Dynamics Simulations. *Chem. − Eur. J.* **2015**, *21*, 4049−4055.

DOI: 10.1021/acs.jpcb.7b10005
J. Phys. Chem. B 2018, 122, 3339−3353